# EES Catalysis

## Accepted Manuscript

This article can be cited before page numbers have been issued, to do this please use: S. Brundiers, P. Trinke, S. Geiger, V. Gracia-Medrano-Bravo, M. Hubka, J. Ilsemann, B. Bensmann and R. Hanke-Rauschenbach, *EES Catal.*, 2026, DOI: 10.1039/D6EY00106H.

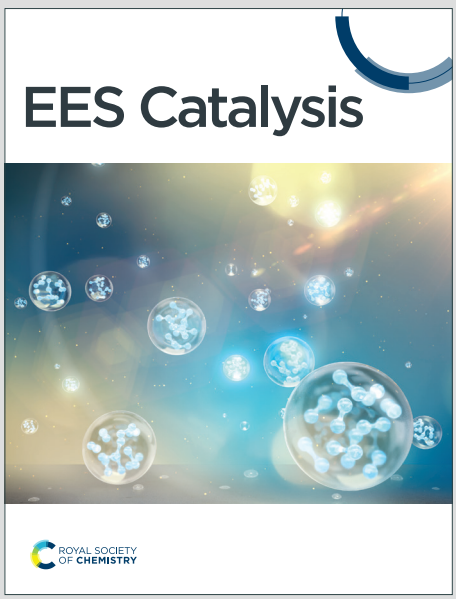




ROYAL SOCIETY OF CHEMISTRY

View Article Online
DOI: 10.1039/D6EY00106H

**Broader Context:**

The transition to a climate-neutral energy system requires technologies that convert renewable electricity into scalable, storable energy carriers. Green hydrogen is central to this transition, enabling sector coupling across industry, mobility, and long-term energy storage. Proton exchange membrane water electrolysis (PEMWE) is particularly attractive due to its dynamic operation, high power density, and hence a good compatibility with fluctuating renewable energy sources. For large-scale deployment, PEMWE must operate safely and efficiently under industrially relevant conditions. High-pressure operation is a key enabler, as it reduces downstream compression requirements and system complexity. However, it increasingly exposes safety-critical gas crossover, especially at low current densities. Managing gas crossover is therefore essential for defining safe operating windows and ensuring long-term reliability. Gas recombination catalysts (GRCs) offer a promising mitigation strategy, yet systematic long-term crossover data under realistic conditions remain scarce, particularly for comparisons between different catalyst configurations. By providing time-resolved insight into the evolution of GRC performance, this work addresses a key knowledge gap at the interface of materials durability, operational safety, and system design.



View Article Online
DOI: 10.1039/D6EY00106H

Journal Name

ARTICLE TYPE

Cite this: DOI: 00.0000/xxxxxxxxxx

# Time-Resolved Performance and Stability of Different Gas Recombination Catalysts in PEM Water Electrolysis†

Steffen Brundiers[a], Patrick Trinke[a], Simon Geiger[b], Victor-Alfonso Gracia-Medrano-Bravo[b], Marek Hubka[b], Jan Ilsemann[b], Boris Bensmann*[a] and Richard Hanke-Rauschenbach[a]

Received Date
Accepted Date

DOI: 00.0000/xxxxxxxxxx

Proton exchange membrane (PEM) water electrolysis is a key technology for large-scale green hydrogen production. However, operation at elevated cathode pressure is increasingly limited by safety-critical gas crossover. While membrane-integrated gas recombination catalysts (GRCs) are widely proposed to master this challenge, their time-dependent performance and stability under realistic operating conditions remain poorly understood. Here, we report a 1,500 hour time-resolved comparative study of three platinum-based GRC configurations (Pt supported on carbon, Pt black, and Pt nanoparticles) operated under identical high-pressure conditions. Despite identical Pt loadings, the investigated systems exhibit markedly different measurable hydrogen in oxygen values, demonstrating that GRC effectiveness is governed by the catalyst configuration rather than Pt loading alone. Post-mortem cross-section analyses reveal pronounced changes in the Pt spatial distribution for the Pt/C system, characterized by an apparent depletion of Pt at the original GRC layer position and the occurrence of a band-like Pt-enriched region within the membrane. Across all GRC systems, measurable hydrogen in oxygen values increase predominantly during the first 250 h of operation, accounting for the majority of the total rise and defining a pronounced run-in period. The evolution of open-circuit voltage decay closely correlates with this behavior, indicating its potential as a non-invasive diagnostic marker. Overall, the results highlight that material-dependent performance evolution, rather than Pt loading alone, governs the long-term effectiveness of membrane-integrated GRC layers. These findings provide indications relevant to the design of resource-efficient and durable GRC concepts for safe high-pressure PEM water electrolysis.





## 1 Introduction

Proton exchange membrane (PEM) water electrolysis is a promising route for renewable hydrogen production because it enables operation under intermittent conditions and at elevated cathode pressures. High-pressure operation increases efficiency by reducing or eliminating mechanical compression requirements in the low-pressure regime (<30 bar). As a result, compression is confined to the subsequent pressure stages if higher hydrogen supply pressures are required. However, pressurized operation introduces the critical challenge of gas crossover: hydrogen permeates to the anode and oxygen to the cathode, especially when thin membranes are used to improve electrochemical performance.[8–10] This not only decreases hydrogen yield but also creates safety risks, as hydrogen concentrations exceeding 4 vol.% in oxygen form explosive mixtures.[11,12] The risk is highest at low current densities, where limited oxygen evolution increases the relative impact of hydrogen crossover. As a result, the operational window of high-pressure PEM electrolyzers is often restricted in the direction of the low current density region, requiring shutdown once critical hydrogen in oxygen ratios are approached. To ensure safe and efficient operation, the hydrogen content in the oxygen stream must therefore be kept below safety-critical levels, for example through thicker membranes, external recombination devices, or gas recombination catalyst (GRC) layers integrated into the catalyst-coated membrane (CCM).[13,14] Deploying platinum-based GRC layers inside the membrane has become a promising strategy, drawing significant attention from both academia and industry.

Platinum-based GRC layers catalyze the recombination of permeating hydrogen and oxygen to water within the membrane. Consequently, they do not reduce the crossover fluxes leaving the

[a] Institute of Electric Power Systems, Leibniz University Hannover, 30167 Hannover, Germany; E-mail: boris.bensmann@ifes.uni-hannover.de
[b] Quest One GmbH, 22143 Hamburg, Germany

† Supplementary Information available: Detailed descriptions of experimental methods, supporting results and discussion, and supporting figures. See DOI: 00.0000/00000000.

View Article Online
DOI: 10.1039/D6EY00106H

Table 1 Overview and comparison of this work with currently available publications in the area of GRC stability testing. Cathode pressure data always refers to the highest measured pressure in the publication, and membrane thickness data always refers to the thinnest measured membrane.

| | crossover comp. to ref. w/o GRC | test duration > 1000 h | continuous $H_2$ in $O_2$ data | cath. pressure >25 bar | mem. thickn. < 180 µm | comp. of multi. diff. GRC materials |
|---|---|---|---|---|---|---|
| Zhang et al.[1] (2022) | ✓ | ✗ (100 h) | ✗ | ✗ (11 bar) | ✓ (~50 µm) | ✗ |
| Stähler et al.[2] (2022) | ✓ | ✗ (250 h) | ✓ | ✗ (amb) | ✓ (~35 µm) | ✗ |
| Klose et al.[3] (2018) | ✓ | ✗ (250 h) | ✓ | ✗ (amb) | ✗ (~204 µm) | ✗ |
| Xie et al.[4] (2025) | ✓ | ✗ (500 h) | ✗ | ✗ (5 bar) | ✓ (~60 µm) | ✗ |
| Mirshekari et al.[5] (2021) | ✗ | ✓ (3,000 h) | ✗ | ✓ (28 bar) | ✗ (~205 µm) | ✗ |
| Zeng et al.[6] (2025) | ✓ | ✓ (3,000 h) | ✓ | ✓ (28 bar) | ✗ (~205 µm) | ✗ |
| Ouimet et al.[7] (2020) | ✓ | ✓ (5,000 h) | ✗ | ✓ (28 bar) | ✗ (~180 µm) | ✗ |
| *This work* | ✓ | ✓ (1,500 h) | ✓ | ✓ (30 bar) | ✓ (~140 µm) | ✓ |

respective catalyst layers into the membrane, but rather decrease the fraction of crossover gases that reaches the opposing electrode. Compared to alternative mitigation strategies, GRC layers offer several advantages, including scalable fabrication, the absence of additional balance-of-plant components, reduced hydrogen in oxygen levels within the cell or stack (which may also mitigate electrode degradation), as well as encouraging experimental and modeling evidence with respect to efficiency and durability.[2,15,16] While most work focuses on GRC layers embedded within the membrane, some studies have explored GRC additives located inside or directly on the anode catalyst layer.[17–20] The present study primarily examines GRCs placed within the membrane, where the catalyst is protected from the harsh anode environment. Such membrane-embedded GRCs have now become a key topic of ongoing development efforts, with several studies on this concept already published.

Initial studies by Klose et al. demonstrated that GRC layers substantially reduce measurable hydrogen in oxygen concentrations at the anode.[3] Subsequent work explored various manufacturing processes, including spray coating,[3] reactive spray deposition technology,[5] and slot-die coating for larger-scale production.[2]

Further studies examined design parameters to increase GRC effectiveness. Garbe et al. compared Pt-doped membranes with membranes containing a defined GRC layer.[16,21] Martin et al. showed that positioning the GRC layer near the anode side is most effective.[22] Abbas et al. investigated the effect of Pt loading,[23] while Zeng et al. studied dual GRC layer configurations.[6]

In these studies, a wide range of GRC configurations have been explored. Platinum nanoparticles remain the most common choice.[3,7,22,23] However, recent publications have also investigated more advanced systems. Xie et al. used an enhanced process that yielded highly dispersed Pt nanoparticles at very low loadings (0.002 mg $cm^{-2}$).[4] Z. Zhang et al. incorporated cerium–zirconium oxide as radical scavengers to counteract the accelerated fluoride release rate (FRR) and membrane degradation that occur when GRCs inside the membrane are used.[1,24] R. Zhang et al. studied Pt–$CeO_2$ nanoparticles supported on carbon nanotubes.[25] Stähler et al. and Smith-Lewis and Litster investigated Pt supported on carbon in the GRC layer.[2,26] To evaluate the practical viability of these different systems, some studies also conducted long-term stress tests, as stable GRC layers are critical for commercial applications requiring extended membrane lifetimes.

Even with this recent progress, comprehensive long-term experimental data on hydrogen in oxygen performance remains extremely limited in the literature, both with and without GRC layers. This lack of data introduces substantial uncertainty in predicting how the hydrogen in oxygen content develops over time. For example, Anschütz et al. observed a "run-in" phase during the first few hundred hours of operation, indicating that hydrogen in oxygen data can change substantially with prolonged operation.[27] Long-term datasets are particularly important for GRC-containing CCMs, as the degradation rates of GRC layers under realistic operating conditions remain largely unknown. Table 1 provides a visual summary of currently available publications in the area of GRC stability testing (test durations $\geq$ 100 h) and compares them to this work. It can be seen that most existing studies with long-term GRC measurements have investigated durations of less than 500 h and only at lower cathode pressures, leaving open knowledge gaps for practical applications. The few publications reporting test durations exceeding 500 h under high cathode pressure conditions do not provide continuous, or in some cases any, measurable hydrogen in oxygen data, as they primarily focus on stability with respect to electrochemical performance. In addition, all of these long-term studies are conducted with relatively thick membranes, often based on Nafion® N117. Lastly, none of the existing studies compares different GRC configurations with respect to their long-term stability. Comprehensive summaries of additional GRC studies are available in the publications of Fahr et al.[28] and Guan et al.[14]

Overall, this literature survey highlights the strong focus on design strategies for reducing measurable hydrogen in oxygen values in the anode exhaust gas using Pt-based GRC systems. However, because studies employ different test benches, cell architectures, and operating conditions, comparisons between different GRC materials remain difficult. Even when long-term data are available, they often lack continuous time-resolved measurable hydrogen in oxygen values that could reveal degradation mechanisms (see Table 1). Consequently, the long-term evolution of hydrogen in oxygen values in the anode exhaust gas is still poorly characterized, both with and without GRC layers incorporated into the membrane. Open questions remain regarding whether the hydrogen to oxygen ratio in the anode exhaust gas increases or decreases over time, whether GRC activity decays, and how GRC layer degradation manifests. These uncertainties are critical because a sudden rise in hydrogen in oxygen values may require

View Article Online
DOI: 10.1039/D6EY00106H



system shutdown for safety reasons, even when electrochemical performance appears unaffected.

To address these gaps, the present study investigates three distinct Pt-based GRC systems alongside a reference membrane without a GRC layer. Electrochemical characterization, hydrogen in oxygen measurements, and ex-situ imaging are combined, with all CCMs tested under identical conditions (same electrodes, test bench, cell configuration, and protocol) to enable a direct comparison of material-system-dependent behavior. In addition to initial characterization, 1,500 h of long-term testing under industry-relevant conditions, including elevated pressure, dynamic load cycles, and shut-down conditions, are reported, providing a basis for analyzing the temporal evolution of performance and the effectiveness of the implemented measures in reducing the net detectable hydrogen content in the oxygen outlet. The complete dataset underlying this study, comprising time-resolved electrochemical measurements for all investigated systems, is openly available via Zenodo.[29] This enables full reproducibility of the presented analyses and facilitates further use in modeling or benchmarking studies.

The remainder of this paper is organized as follows. Section 2 details the materials, experimental setup, and measurement protocol. Subsequently, scanning electron microscopy (SEM) images acquired at the beginning of test (BoT) and end of test (EoT) are analyzed. Furthermore, all samples are compared with respect to their electrochemical performance and the extent to which the implemented measures reduce the net detectable hydrogen content in the oxygen outlet at BoT and EoT. Finally, the time-resolved cell behavior during long-term stress testing is examined, including an evaluation of the evolution of the measurable hydrogen in oxygen values and open-circuit voltage trends.

## 2 Experimental

The experimental section is divided into four parts. First, the manufacturing process of the investigated CCMs is described. This is followed by a presentation of the test cell and its assembly. Subsequently, the test bench and all additional measurement devices are outlined. Finally, the test protocol and measurement conditions are stated. This section is kept as compact as possible, and additional information on the experimental procedures can be found in the Supporting Information (SI).

### 2.1 Manufacturing of CCMs and GRC layers

The CCMs under investigation were manufactured by Quest One GmbH (Hamburg, Germany). In total, four different CCMs were evaluated: three containing a GRC layer and one reference CCM without a GRC layer. The fabrication procedure for the GRC layer is similar to that described by Stähler et al.[2] (further details are provided in Section S.1 of the SI). All CCMs are based on a Nafion® N115 membrane. For each of the three GRC samples, the general structure can be conceptualized as a five-layer CCM, as shown in Figure 1. From top to bottom, it consists of the cathode catalyst layer, the Nafion® N115 membrane, the GRC layer, a protective layer, and the anode catalyst layer. This configuration places the GRC layer near the anode, which has been identified as the most effective position.[22]

Table 2 Overview of analyzed catalyst configurations used in the GRC layer (additional information in Section S.1 in the SI).

| Identifier | Supplier | Comment |
|---|---|---|
| PtNano | ChemPUR | commonly used; high surface area |
| PtBlack | BASF | high surface area due to porous structure |
| Pt/C | Umicore | Pt supported on carbon for high surface area |
| Reference | – | baseline without GRC or protective layer |

All CCMs containing a GRC layer were manufactured using the same procedure and identical anode and cathode electrodes. The only difference between samples lies in the catalyst configuration used for the GRC layer: platinum nanoparticles (PtNano), platinum black (PtBlack), or platinum supported on carbon (Pt/C). Table 2 provides an overview of all analyzed catalyst configurations. All CCMs with a GRC layer have the same platinum-based GRC loading of 50 $\mu g\ cm^{-2}$, with only the physical form of the platinum differing between samples. The reference sample without a GRC layer consists solely of the Nafion® N115 membrane coated with the anode and cathode catalyst layers. Hence, the GRC and protective layers are absent as outlined in Figure 1.

### 2.2 Test cell and material setup

All measurements were performed in a test cell developed at Leibniz University Hannover at the Institute of Electric Power Systems (IfES). The cell has an active area of 4 $cm^2$ and is equipped with gold-coated titanium end plates and flow fields. Key features include gas tightness up to 30 bar and a design in which the compression force on the electrochemically active area is decoupled from the force used to ensure gas tightness. Additional details on the cell design are provided in Section S.2 of the SI.

The aforementioned CCMs are assembled in this cell along with a porous transport layer (PTL) at the anode and a gas diffusion layer (GDL) at the cathode. On the anode, a sintered titanium fiber PTL with a thickness of 1 mm and a porosity of 56% is used (Bekaert, Belgium). This PTL is additionally coated with iridium via sputter coating with a 50 nm coating thickness. Iridium is used instead of the commonly applied Pt coating to reduce the amount of hydrogen recombining at the anode PTL, ensuring that the hydrogen crossover flux calculated from the measured hydro-

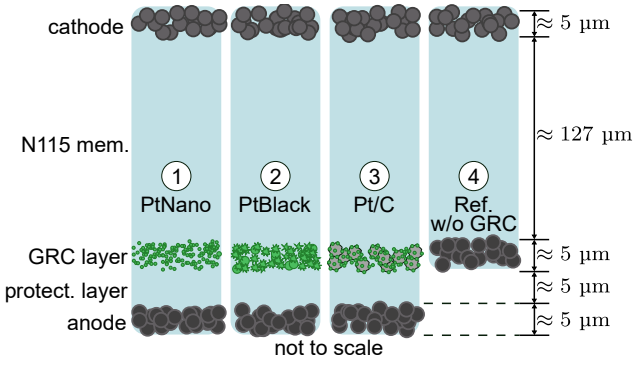


Fig. 1 Schematic structure of the investigated CCMs: 1) PtNano, 2) PtBlack, 3) Pt/C, and 4) reference without GRC layer (not to scale). See Section S.1 of the SI for fabrication details.

View Article Online
DOI: 10.1039/D6EY00106H



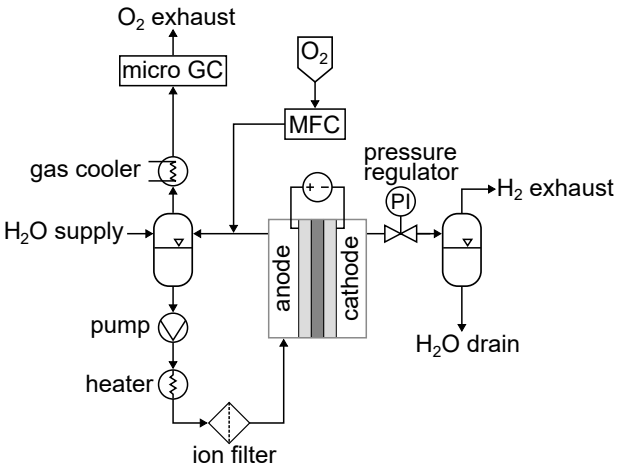


Fig. 2 Schematic of the PEM water electrolysis test bench including pressure control and anode exhaust gas analysis.

gen in oxygen values more closely reflects the actual hydrogen crossover reaching the anode side.[30] On the cathode, a carbon paper GDL with a thickness of 210 μm and with hydrophobic treatment (E20H, Freudenberg, Germany) is used.

### 2.3 Test bench setup and measurement devices

All measurements were carried out on an in-house built eight-channel test bench at IfES at Leibniz University Hannover (see Figure S.1d in the SI). Figure 2 schematically illustrates one representative channel. The system supplies the cell with ultrapure water at 80 °C and a conductivity below 0.2 μS $cm^{-1}$ (see Figure S.8 in the SI). Conductivity is monitored continuously, and water purity is maintained with an in-line ion-exchange filter. Water is fed exclusively to the anode side in a closed loop and circulated via a peristaltic pump (Shenchen Drifton Lab S3) at 80 ml/min.

The anode operates at ambient pressure, while the cathode pressure is regulated using a back-pressure regulator (Equilibar ZF-Series) controlled via a PCS-DRP70 pressure controller (Specken Drumag, Germany). Electrochemical measurements were performed using a BCS-815 (BioLogic, France). Gas analysis was conducted with a gas chromatograph (990 microGC, Agilent; nitrogen as carrier gas), supplied with gas drawn from the anode tank. Prior to analysis, the gas is cooled to 5 °C using a gas cooler (ECP2000C, M&C Techgroup, Germany) to remove moisture.

To ensure safe operation below the lower explosion limit and provide sufficient flow for gas analysis, the anode outlet gas stream is diluted with oxygen. A constant oxygen dilution flow of 0.03 g/min is added using a mass flow controller (EL-FLOW Prestige FG-201CV, Bronkhorst, Netherlands) directly downstream of the cell. As a result, a correction is required to determine the actual hydrogen in oxygen concentration at the cell outlet and to calculate the apparent hydrogen crossover flux from the value measured at the gas chromatograph following Martin et al.[31]

It is important to emphasize that this measurement approach does not provide direct access to the intrinsic hydrogen crossover flux through the membrane, but rather detects only the fraction of hydrogen that leaves the cell and reaches the gas chromatograph. Consequently, the measured hydrogen in oxygen signal represents a composite quantity that reflects the interplay of multiple processes. These include (i) the intrinsic hydrogen permeation from the cathode into the membrane, (ii) recombination and electrochemical consumption processes within the membrane, (iii) additional recombination or hydrogen oxidation at the anode catalyst layer and the porous transport layer (PTL), and (iv) coupled transport–reaction phenomena within the membrane.

Even in the reference case without a GRC layer, the hydrogen flux detected at the anode outlet is therefore expected to be lower than the actual hydrogen crossover flux entering the membrane from the cathode. A fraction of the permeating hydrogen is consumed before reaching the outlet, for example by recombination or hydrogen oxidation at the anode catalyst or the PTL coating. As a result, crossover fluxes derived from hydrogen in oxygen measurements represent a lower bound of the true crossover. This limitation is well known and currently inherent to state-of-the-art measurement approaches.[32,33]

In the presence of a GRC layer, the interpretation becomes more complex. The incorporation of a recombination catalyst within the membrane introduces an additional reaction zone, in which permeating hydrogen and oxygen can be converted to water before reaching the anode. As a consequence, the hydrogen flux entering the membrane from the cathode, the flux within the membrane, and the flux reaching the anode can differ significantly. In addition to recombination, structural effects such as modified diffusion pathways or increased transport resistances (e.g., in Pt/C-based systems) may further influence the measurable signal, although this remains a possible hypothesis rather than a confirmed mechanism.

A rigorous separation of these contributions into intrinsic transport and kinetic effects requires a detailed reaction–diffusion modeling framework, including microkinetic descriptions of the recombination reaction, transport properties of the membrane, and spatially resolved concentration profiles. However, such models are currently not sufficiently constrained by experimental data and may lead to non-unique parameter sets. Therefore, a quantitative decomposition of the measured signal is beyond the scope of the present work.

Instead, the present study adopts an integral perspective and evaluates the overall effectiveness of different GRC configurations based on the measurable hydrogen in oxygen signal under identical operating conditions. This approach inherently captures all relevant contributions, including recombination, transport, and structural effects, and is therefore directly relevant for practical applications. While this does not allow attribution of the observed behavior to individual mechanisms, it enables a consistent and comparative assessment of the functional performance of different GRC systems. Furthermore, from a practical application perspective, the safety aspect is of primary importance. In this context, the key parameter is the integral hydrogen in oxygen concentration downstream of the cell or stack, which must be minimized. Consequently, this parameter represents the main focus of the present study.

It is further assumed that contributions from anode-side recombination processes are comparable across all samples, as identical

View Article Online
DOI: 10.1039/D6EY00106H



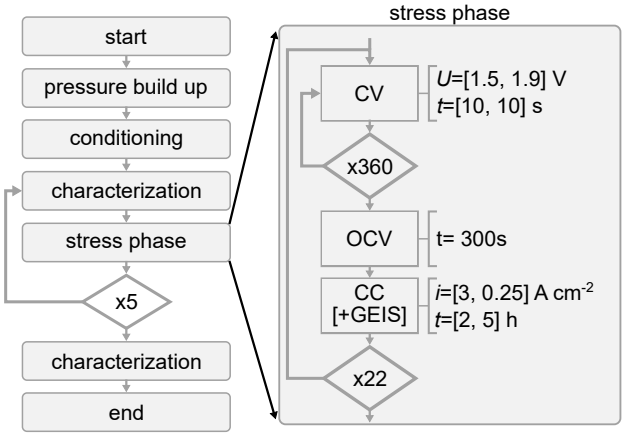


Fig. 3 Experimental protocol comprising pressure build-up, conditioning, characterization, and stress phases. Details of the stress phase are shown on the right. Comprehensive descriptions of all phases are provided in Section S.3 of the SI.

anode materials and operating conditions are employed. Differences in the measured hydrogen in oxygen signal are therefore primarily attributed to the presence and properties of the GRC layer.

### 2.4 Test conditions and protocol

The CCM is assembled in a dry state together with the PTL and GDL described in Subsection 2.2. A compression force of 1.4 kN is applied, and the cell is connected to the test bench. Before measurements begin, thermal conditioning and membrane wetting are performed: water at 80 °C and 80 ml/min is supplied to the anode for one hour, while the cathode remains dry. Subsequently, the electrochemical protocol shown in Figure 3 is initiated. A detailed description of each measurement phase is provided in Section S.3 of the SI.

During the pressure build-up phase, constant-current steps are applied to increase the cathode pressure via hydrogen production. After reaching 30 bar absolute, the compression force is increased to 2.37 kN. After 15 min, the compression force is checked to compensate for mechanical settling. Throughout the experiment, the pressure of the anode side is not controlled, resulting in a pressure close to ambient.

The conditioning phase consists of 30 min at 0.2 A $cm^{-2}$, 30 min at 0.5 A $cm^{-2}$, and 19 h at 1.9 V constant voltage. The main part of the measurement then begins, comprising recurring alternations between stress and characterization phases. The initial characterization phase is performed twice to ensure reliable BoT characterization.

Each characterization phase includes a polarization curve with galvanostatic electrochemical impedance spectroscopy (GEIS) at each current density, a hydrogen in oxygen measurement at selected current densities, and another polarization curve with GEIS. Each full characterization phase lasts approximately 29 h.

The subsequent stress phases last approximately 235 h and consist of the steps shown in Figure 3. First, voltage jumps between 1.5 V and 1.9 V are applied with 10 s holds for a total of 2 h, corresponding to 360 cycles. These voltage cycles are expected to alter the potential distribution at the platinum sites in the GRC layer and induce stress. Next, the current is shut off for 5 min and the open-circuit voltage (OCV) decay is recorded. This deliberately creates a hydrogen oversupply due to the differential pressure, causing the overall cell potential to drop below the electrolysis voltage (≈1.4 V), which is intended to further stress the GRC layer. Finally, two constant-current holds are applied: 2 h at 3.0 A $cm^{-2}$ and 5 h at 0.25 A $cm^{-2}$, each followed by a GEIS measurement. These holds simulate extended high-load and part-load operation and allow monitoring of voltage, hydrogen in oxygen values, and high-frequency resistance (HFR) over time.

After six cycles of characterization and stress phases (corresponding to a total test duration of 1,500 h), an EoT characterization identical to the BoT characterization is performed. In addition to the electrochemical measurements, ex-situ focused ion beam–scanning electron microscopy (FIB–SEM) images were taken at BoT using an unused sample and on the stressed samples after 1,500 h of operation.

## 3 Results and Discussion

The experimental results and discussion are divided into four sections. First, SEM images of the CCM samples acquired at BoT and EoT are examined to assess the manufacturing quality of the CCMs and their apparent degradation. Next, the overall performance of each sample is evaluated by comparing its electrochemical behavior and its ability to reduce the net detectable hydrogen content in the oxygen outlet at BoT and EoT. Finally, the temporal evolution of measurable hydrogen in oxygen values and open-circuit voltage decay is analyzed to gain deeper insight into time-dependent degradation trends.

### 3.1 SEM cross-sections

Figure 4 shows the BoT and EoT SEM cross-sections of the GRC layer, protective layer, and anode catalyst layer, together with the corresponding EDX signals of Ir and Pt. The BoT samples represent pristine material that was manufactured but never assembled into the cell or exposed to mechanical load or water. Additional SEM images and methodological details of the ex-situ analysis are provided in Section S.4 of the SI.

The analysis begins with the PtNano BoT sample in Figure 4a. The Pt nanoparticles in the GRC layer appear significantly agglomerated or are inherently larger than the nominal material specification, as they fall in the micrometer range despite the manufacturer-stated average particle size of 0.1 µm. Furthermore, the dispersion is highly non-uniform, with pronounced particle clustering. The protective layer between the anode and GRC layer is comparatively thin at approximately 3 µm. Regarding the EDX data, a slightly more intense Pt signal compared to the background noise is visible within the anode catalyst layer, although this may also result from overlap with the Ir signal. The Pt and Ir signals detected in the pure membrane are at or near the detection limit of the EDX technique at such low concentrations. Accordingly, these signals are not interpreted as evidence of Pt presence in the membrane, but rather as background noise. The total CCM thickness is around 138 µm ± 2 µm. For the EoT sam-

View Article Online
DOI: 10.1039/D6EY00106H

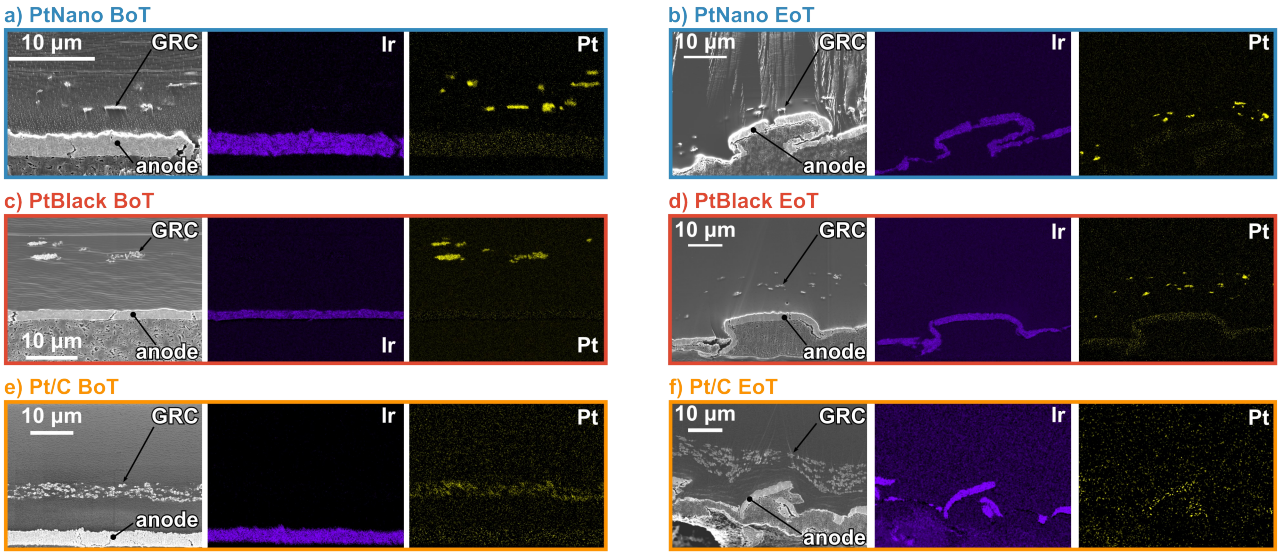


Fig. 4 Close-up ex-situ cross-section imaging of the anode region of all samples with GRC layers at BoT and EoT (1500 h): PtNano (a,b), PtBlack (c,d), and Pt/C (e,f), including corresponding Ir (purple) and Pt (yellow) EDX maps. Information on the methodological process of the ex-situ analysis is given in Section S.4 of the SI.

ple in Figure 4b, severe deformations are observed on the anode side. These correspond to swelling or creep of the CCM into the PTL pores. The dimensions of the deformation align with the pore and fiber dimensions of the fiber-felt anode PTL. This effect is enhanced by the dry-state assembly, where the membrane expands upon water exposure and is pressed into the already compressed PTL. Notably, even after 1,500 h of operation and despite the thin protective layer, no substantial Pt loss or restructuring is evident, as a large fraction of GRC particles remains in its original location. The GRC particle clusters remain near the anode in a distinct layer. After the test, the overall CCM thickness is approximately 125 µm ± 6 µm.

For the PtBlack BoT sample in Figure 4c, relatively large Pt particles are visible in the GRC layer, ranging from 0.5 µm to 5 µm. These particles exhibit porous and rough surface structures, as also shown in the close-up images in Section S.4 of the SI. The particles appear in clusters rather than forming a uniform dispersion. Compared to the PtNano sample, a noticeably thicker protective layer (approximately 9 µm) is present between the anode and the GRC layer. The total CCM thickness is about 155 µm ± 3 µm. EoT images in Figure 4d again reveal deformation effects similar to those observed in the PtNano case. Large Pt particle clusters remain near the anode, indicating that a substantial amount of Pt persists after 1,500 h in the original location. The post-test CCM thickness is approximately 143 µm ± 6 µm.

For the Pt/C BoT sample, the GRC layer exhibits a highly uniform and comparatively dense morphology (Figure 4e). As expected from the incorporation of carbon support particles, a larger number of foreign particles is observed relative to the other GRC layers despite identical Pt loading. The protective layer thickness is approximately 6 µm, while the total CCM thickness amounts to 148 µm ± 2 µm.

In strong contrast to the other samples, the EoT cross-section of the Pt/C GRC layer (Figure 4f) exhibits a markedly elemental composition. SEM–EDX mapping reveals a pronounced depletion of Pt at the position originally occupied by the GRC layer. At the same time, the electron micrograph still shows the characteristic structural features of the carbon support, indicating that the carbon matrix largely remains intact while the Pt distribution has changed significantly. To further substantiate these observations, additional high-magnification EDX images of the BoT and EoT Pt/C GRC layers were acquired and are shown in Figure S.5 of the SI. These results likewise show no indication of residual Pt within the GRC layer at EoT. In addition, a distinct relocation of ruthenium (Ru), a component of the anode catalyst, is observed in high-magnification EoT Pt/C samples. Notably, Ru signals are detected exclusively at the outer boundary of the carbon matrix facing the anode. To validate this observation, a larger area of the EoT Pt/C sample was reanalyzed; within this region, no significant Ru accumulation at the GRC layer is detected. This indicates that Ru deposition is scarce and found only locally rather than uniformly distributed across the GRC layer. Moreover, such Ru signals are not observed in any other GRC layer (see Figure S.5 in the SI), suggesting that the carbon matrix may act as a localized trapping interface for migrating Ru species. Therefore, Ru migration is not expected to significantly influence the main results of this study, as it is not detectable in PtNano and PtBlack samples and is only observed sporadically in Pt/C. This observation is included for completeness.

To further examine the apparent redistribution of Pt and to explore its possible spatial relocation within the CCM, additional SEM–EDX analyses were performed across the full EoT membrane cross-section with a CCM thickness of approximately 150 µm ± 5 µm (Figure 5). These measurements also highlight the intrinsic limitations of SEM–EDX for resolving highly dispersed or low-concentration elemental distributions over large cross-sectional areas. In the electron image (Figure 5a), faint bright features forming a band-like region can be discerned. Correspondingly, a

View Article Online
DOI: 10.1039/D6EY00106H



slightly elevated Pt signal is detectable in the associated EDX map (Figure 5b), albeit close to the sensitivity limit of the technique. Owing to the limited spatial resolution, these data do not allow quantitative tracking of Pt transport or reliable determination of Pt concentration gradients across the membrane.

To confirm the chemical identity of these features, selected particles within the band-like region were analyzed at higher magnification (Figure 5c). The corresponding EDX spectra unambiguously identify these particles as Pt. Variations in the measured Pt wt.% are attributed to differences in particle depth within the membrane as well as to geometric effects related to the interaction volume of the EDX acquisition. Notably, comparable Pt-containing features were not detected in any BoT samples and are also absent in the EoT reference CCM without a GRC layer. This observation makes an origin from the initially introduced Pt/C GRC material plausible, but it does not prove the source of the Pt-containing species or the pathway by which they accumulated within the membrane.

Based on the present SEM–EDX analysis, a pronounced redistribution of Pt is evident only for the Pt/C system. However, the absence of comparable features in the other samples does not preclude similar processes occurring at lower rates or below the detection limit of SEM–EDX. The limited sensitivity and spatial resolution of this technique prevent a quantitative assessment of Pt transport across the full membrane thickness. Similar limitations have been reported in recent work by Zeng et al., who observed subtle Pt dissolution and redeposition effects for dual Pt-based GRC layers, detectable only in close proximity to the original GRC layer and at very high magnification.[6]

Based on the observed spatial redistribution and previous findings from the fuel cell literature, a physically consistent working hypothesis, rather than a directly proven mechanism, may involve a sequence of Pt dissolution, ionic transport through the membrane, and subsequent redeposition of Pt.[34–37] In this framework, Pt is assumed to dissolve under local electrochemical conditions into ionic Pt species, particularly during transient operating conditions such as potential cycling or OCV phases.[34,37] Then, the dissolved Pt species can potentially migrate through the hydrated membrane phase in ionic form.[34,36] A transport of metallic Pt particles appears unlikely, as the particle dimensions are substantially larger than the characteristic dimensions of the hydrated membrane transport pathways reported in the literature.[36] The migration of dissolved Pt species may be generally described by diffusion and electrochemical transport processes within the membrane.[34–36] Redeposition is then assumed to occur preferentially in regions where reducing conditions are present. In particular, hydrogen crossover has been proposed as a key factor that may promote Pt reduction and Pt-band formation inside the membrane.[35,36] Once initial Pt nuclei are formed, further Pt accumulation and particle growth may occur locally, which could explain the experimentally observed Pt-enriched regions.[34,36]

Processes of this type have been extensively discussed in the PEM fuel cell literature and provide a reasonable first-order approximation for interpreting the present observations, even though the specific operating conditions and local potential distributions differ from those in PEM fuel cells.[37] However, it should be emphasized that the present study does not provide direct experimental evidence to unambiguously distinguish between the contributing mechanisms, such as electrochemical dissolution and redeposition, Ostwald ripening, or other transport-driven redistribution processes. The proposed mechanism should therefore be regarded as a physically consistent hypothesis rather than a definitive explanation. A detailed mechanistic investigation, including targeted experiments and advanced characterization, is beyond the scope of the present work and is subject of ongoing studies.

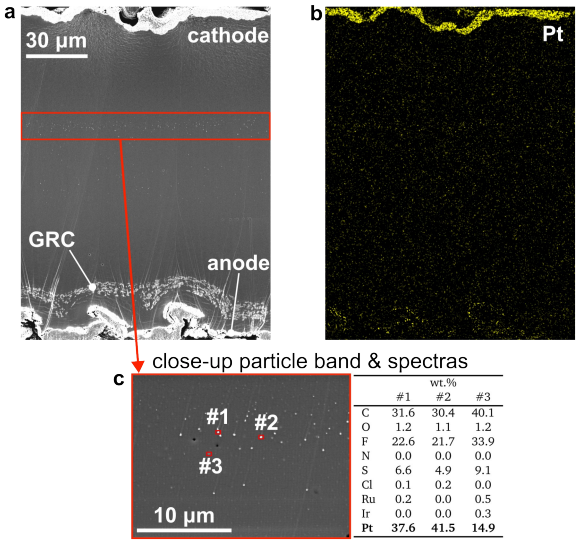


| | wt.% | | |
|---|---|---|---|
| | #1 | #2 | #3 |
| C | 31.6 | 30.4 | 40.1 |
| O | 1.2 | 1.1 | 1.2 |
| F | 22.6 | 21.7 | 33.9 |
| N | 0.0 | 0.0 | 0.0 |
| S | 6.6 | 4.9 | 9.1 |
| Cl | 0.1 | 0.2 | 0.0 |
| Ru | 0.2 | 0.0 | 0.5 |
| Ir | 0.0 | 0.0 | 0.3 |
| **Pt** | **37.6** | **41.5** | **14.9** |

Fig. 5 Ex-situ cross-section imaging of the full CCM cross-section of the Pt/C sample after 1,500 h: (a) electron image, (b) Pt EDX map, and (c) close-up image of the particles in the CCM, with corresponding EDX spectra showing that the particles are platinum.

The pronounced change in Pt distribution observed for the Pt/C system, compared to the PtBlack and PtNano samples, may be related to structural differences between the catalyst configurations (see Section S.1 in the SI for more information on the GRC parameters). In the Pt/C system, Pt is present as highly dispersed particles on a porous high-surface-area carbon support, resulting in substantially smaller Pt particle sizes and significantly higher electrochemically accessible Pt surface area compared to the unsupported PtNano and PtBlack systems. This morphology provides a larger interfacial area between Pt and membrane and a higher fraction of small, highly exposed Pt particles, which could increase the susceptibility to Pt dissolution and subsequent transport of Pt-containing species. However, this interpretation remains only a plausible hypothesis rather than a direct conclusion from the present SEM-EDX data. In addition, dissolution from many finely dispersed Pt sites may lead to a more spatially coherent redeposition pattern, whereas redistribution from larger PtBlack or PtNano agglomerates may remain more localized, weaker, or masked by Pt remaining at the original GRC layer position. Literature investigations on comparable Pt/C catalyst systems further showed that Pt particles located on the exterior carbon surface are particularly susceptible to degradation via Ostwald ripening, agglomeration, dissolution, and redeposi-

View Article Online
DOI: 10.1039/D6EY00106H



tion processes.[38] In contrast, the larger and more agglomerated Pt structures in the PtBlack and PtNano systems provide lower effective Pt surface area and are therefore expected to exhibit lower Pt mobility and reduced susceptibility to redistribution processes.

Hence, although similar redistribution processes may also occur in the PtBlack and PtNano samples, they are likely to proceed at substantially lower rates and may therefore remain below the detection limit of SEM–EDX. Accordingly, while the present results suggest a configuration-dependent Pt mobility, a quantitative structure–mobility relationship cannot be established based on the available data and requires dedicated investigation which is part of currently ongoing work.

Consequently, while the present results provide qualitative evidence for Pt redistribution phenomena in membrane-embedded GRC layers, advanced spatially resolved characterization techniques will be required to elucidate the underlying transport mechanisms and quantify Pt redistribution in detail. High-resolution synchrotron-based XRF has recently been demonstrated as a promising approach for such analyses.[39]

### 3.2 Electrochemical performance

To assess the influence of each GRC additive on the overall electrochemical performance of the cell, each CCM was evaluated based on its BoT and EoT polarization and HFR curves (see Figure 6), recorded during the characterization phases of the measurement protocol. Additional analyses, including Tafel plots and cell-voltage evolution over the 1,500 h stress phase, are presented in Sections S.5 and S.11 in the SI, as the primary focus of this work is the influence of the GRC layers on the net detectable hydrogen content in the oxygen outlet, discussed in the next section.

The BoT data shown in Figure 6a and c indicate that all CCMs exhibit similar electrochemical performance at BoT. At 0.2 A cm$^{-2}$, cell voltages ranged between 1.55 V and 1.56 V, while at 2.5 A cm$^{-2}$ the range broadened to 1.96–2.07 V. The PtBlack and PtNano samples show slightly larger deviations in both overall and *iR*-free cell voltages, suggesting possible contamination within the cell or CCM, potentially originating from manufacturing or incomplete conditioning. Over time, this effect diminished, and the cell voltage decreased for these samples. At BoT, the HFR of all samples ranged between 132.36 and 159.29 mΩ cm$^2$, with a slight increase in HFR at higher current densities. PtNano and PtBlack exhibit a more pronounced rise, supporting the contamination hypothesis for these two samples as this is a typical behavior for contaminated CCMs.[40] The reference CCM has the lowest absolute HFR, attributable to its thinner membrane resulting from the absence of GRC and protective layers. PtNano shows the second-lowest HFR, consistent with its thinner protective layer and overall reduced CCM thickness. PtBlack and Pt/C display slightly higher HFR values because they have the greatest overall CCM thicknesses. In the Pt/C case, this may also be linked to the incorporation of a high quantity of foreign support particles in the GRC layer, which could reduce the proton conductivity. Overall, HFR differences at BoT appear to stem primarily from variations in CCM thickness or an initial membrane contamination, while the foreign particles introduced by the GRC layer have a smaller

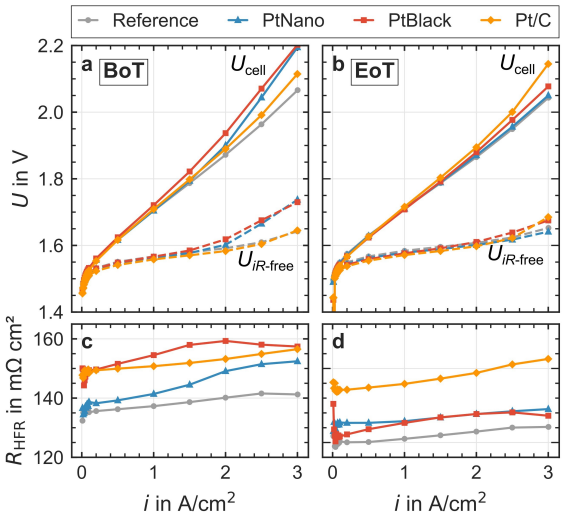


Fig. 6 Electrochemical performance at BoT (a,c) and EoT (b,d) measured at 80 °C and 30 bar absolute cathode pressure; EoT corresponds to approximately 1,500 h of stressed operation: (a,b) Cell voltages ($U_{cell}$, solid lines) and *iR*-free cell voltages ($U_{iR-free}$, dashed lines); (c,d) Corresponding HFR values obtained by electrochemical impedance spectroscopy.

effect. This is supported by the observation that PtBlack, despite containing fewer foreign particles, exhibits an elevated HFR similar to the Pt/C sample at BoT. These findings align with Abbas et al.[23], who reported that GRC layer loading and thus the amount of foreign particles has no significant influence on HFR.

The EoT data after 1,500 h of operation are shown in Figure 6b and d. The polarization curves and *iR*-free voltages converged for all samples, likely because they were fully conditioned and initial contaminants had been removed during operation. At higher current densities, no significant degradation is evident. In fact, cell voltages decreased for all samples except Pt/C, which showed a slight increase at 3 A cm$^{-2}$. At lower current densities, a modest voltage increase between 13 mV and 22 mV at 0.05 A cm$^{-2}$ was observed for all samples, indicating increased activation losses. Similar to the voltage behavior, HFR values also converged and generally decreased compared with the BoT data. This reduction in HFR over time is also evident in Figure S.15 in the SI, which depicts the temporal evolution of the HFR at current densities of 0.25 A cm$^{-2}$ and 3.0 A cm$^{-2}$ over the full 1,500 h. The decrease is likely due to conditioning during long-term operation and the removal of manufacturing-related contaminants. Additionally, settling at the interfaces between the various layers (electrodes, membrane, GRC) may also contribute to the reduction in HFR over time.

Overall, after approximately 1,500 h of operation, no significant changes in the polarization behavior were observed, indicating that the GRC layers remain electrochemically stable. This observation is consistent with previously reported long-term studies, which demonstrate that the incorporation of GRC layers does not lead to substantial electrochemical performance degradation over several thousand hours of operation.[5–7] Instead, performance im-

View Article Online
DOI: 10.1039/D6EY00106H



proved for all samples except Pt/C. The Pt/C sample showed only a small reduction in HFR and a slight voltage increase at higher current densities, likely due to residual losses. These potentially originate in the catalyst layer, with dissolution of the carbon support in the GRC layer contaminating the electrodes as a possible degradation mechanism. In addition, the fact that the HFR of the Pt/C sample does not decrease to the same level as the other samples during the test period may indicate an influence of the Pt/C layer on long-term electrochemical performance, as the thick layer of foreign GRC particles may negatively affect proton conductivity. Hence, only Pt/C shows minor indications of accelerated electrochemical degradation, although even longer testing periods would be required to confirm this.

### 3.3 Characteristics of the measurable hydrogen in oxygen data

GRC layers are generally incorporated into the membrane to lower the hydrogen in oxygen content at the anode and thereby ensure safe and efficient operation of high-pressure PEM water electrolyzers. In this section, the measurable hydrogen in oxygen data of each sample is analyzed. First, the BoT status is analyzed and in a second step compared with the EoT performance over the full current density range, based on data obtained during the characterization phases of the measurement protocol.

Due to limitations in the available CCM material and test-stand capacities, not all long-term tests could be repeated multiple times. However, selected retests were conducted to support the key findings of this work. These retests include the reference, the Pt/C, and the PtNano samples. Their results are referenced at the appropriate points in the main text and are shown in full in Section S.14 of the SI.

#### 3.3.1 Begin of test hydrogen in oxygen data

The BoT hydrogen in oxygen data for all samples is presented in Figure 7. Subfigure (a) shows the measured hydrogen concentration in the oxygen stream at the anode outlet, corrected for $O_2$ dilution. Subfigure (b) presents the corresponding hydrogen crossover flux at the anode outlet. It is likely that the actual hydrogen flux reaching the anode is higher than the value derived from the measured hydrogen in oxygen content. This discrepancy arises because part of the hydrogen undergoes chemical recombination or hydrogen oxidation reaction (HOR) on the anode catalyst or on the PTL coating.[30,32,33] Consequently, the values shown here represent a lower bound of the actual hydrogen crossover flux reaching the anode side. Accordingly, all fluxes derived from hydrogen in oxygen measurements are referred to as apparent hydrogen fluxes and are not interpreted as intrinsic membrane permeation fluxes.

Figure 7c presents a metric $\varepsilon_{GRC}$ that quantifies the relative reduction of the apparent hydrogen flux derived from the hydrogen in oxygen concentration in the anode exhaust gas when a GRC layer is present, as given by Equation 1. This metric does not describe a reduction of the intrinsic membrane permeation flux, but rather the effectiveness of the GRC-containing CCM in lowering the net detectable hydrogen leaving the cell. For brevity, this metric is referred to in the following as the apparent GRC

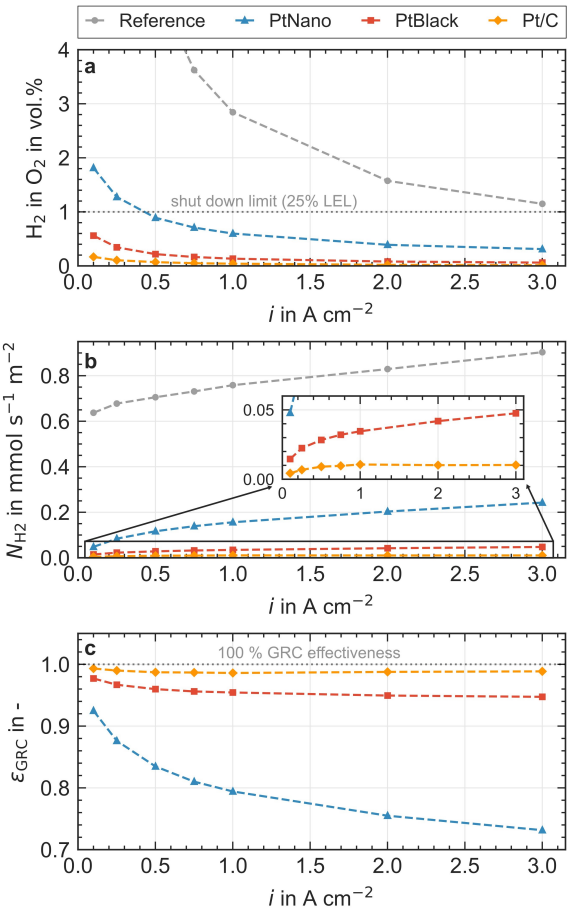


Fig. 7 Gas analysis data of all samples at BoT, measured at 80 °C and 30 bar absolute cathode pressure: (a) dilution-corrected measurable hydrogen in oxygen concentration at the anode outlet; (b) apparent hydrogen flux derived from the anode exhaust gas; (c) apparent GRC effectiveness, defined as ($\varepsilon_{GRC} = 1 - N_{H2}^{cross}/N_{H2,ref}^{cross}$) as defined in Equation 1

.

View Article Online
DOI: 10.1039/D6EY00106H



effectiveness.

$$\varepsilon_{\mathrm{GRC}} = 1 - \frac{N_{\mathrm{H2}}^{\mathrm{cross}}}{N_{\mathrm{H2,ref}}^{\mathrm{cross}}} \quad (1)$$

Here, $N_{\mathrm{H2}}^{\mathrm{cross}}$ denotes the apparent hydrogen crossover flux reaching the anode side when a GRC layer is present, and $N_{\mathrm{H2,ref}}^{\mathrm{cross}}$ is the respective apparent hydrogen crossover flux of the reference sample without a GRC layer. A value of 0 indicates that the hydrogen crossover flux based on the measurable hydrogen in oxygen data in the anode exhaust stream equals that of the reference sample, while a value of 1 signifies that no detectable hydrogen leaves the anode due to recombination or HOR. The detailed recombination and mitigation mechanisms within the GRC layer are not yet fully understood. Hydrogen removal may occur via chemical recombination or via an electrochemical pathway involving HOR and the oxygen reduction reaction (ORR) on the same Pt particle within the GRC layer. Furthermore, an incorporated GRC layer may also alter the transport paths of the crossover species and hence change the detectable hydrogen in oxygen values at the anode exhaust stream. Dedicated experiments are required to gain deeper mechanistic insight both for the recombination kinetics and the local diffusion behavior. However, they are beyond the scope of the present study which is assessing the overall apparent effectiveness of the GRC layer, independent of the underlying mechanism. Nevertheless, improved mechanistic understanding could inform the design of more effective GRC layers and is therefore part of our future work.

From the data in Figure 7, all GRC layers are effective, as the hydrogen in oxygen values and corresponding apparent crossover fluxes in the anode exhaust stream are consistently lower than those of the reference CCM, yielding an apparent GRC effectiveness $> 0$ for all samples. Figure 7a shows that the reference CCM without a GRC layer exhibits hydrogen in oxygen concentrations exceeding the lower explosion limit (LEL) of 4 vol.%. Assuming a shutdown threshold of 1 vol.% (25% of the LEL), such a system would not be permitted to enter operation at all. This highlights the importance of GRC layers for high-pressure operation, even when using relatively thick membranes ($> 127$ µm).

The apparent hydrogen crossover flux in Figure 7b shows the expected increase with current density due to the supersaturation effect, which has been reported in several studies.[19,31,41] The values shown represent the apparent hydrogen crossover flux calculated from the hydrogen in oxygen content leaving the anode exhaust gas stream. Earlier publications have demonstrated that this exhaust-gas crossover stream can differ substantially from the crossover stream entering the membrane from the cathode when a GRC layer is used.[15]

In this context, it is important to distinguish between the intrinsic hydrogen crossover flux entering the membrane from the cathode and the experimentally accessible hydrogen flux detected at the anode outlet. This distinction has already been discussed thoroughly in Section 2.3. It is essential for the interpretation of the data, as the experimentally derived hydrogen crossover flux represents a composite quantity rather than the intrinsic membrane permeation alone. Accordingly, all references to hydrogen crossover in the following refer to the measurable hydrogen flux in the anode exhaust stream. Despite this limitation, the described measurement approach represents the current state of the art and enables a consistent comparison between different samples under identical conditions.

For the GRC samples, substantial differences in the reduction of the net detectable hydrogen content in the oxygen outlet are observed despite identical platinum loadings in the GRC layer. This demonstrates that, in addition to Pt loading, the physical properties of the Pt catalyst configuration within the GRC layer strongly influence recombination activity. Literature most frequently reports Pt nanoparticles as the GRC catalyst system.[3,7,22,23] However, in this study, PtNano displayed the poorest reduction of the net detectable hydrogen content, reaching hydrogen in oxygen concentrations near 2 vol.% at 0.1 A cm$^{-2}$, whereas the other two GRC systems remained far below 1 vol.%. As summarized in Section 1 of the SI, the employed PtNano catalyst system exhibits the lowest specific surface area among the investigated catalyst materials due to its comparatively large average particle size of 100 nm. Therefore, the accessible Pt surface area available for recombination is expected to be substantially lower compared to the highly dispersed Pt/C catalyst system. Due to this unexpectedly poor performance, an additional repeat measurement was performed using a new CCM sample (see Figure S.26 in SI). The repeated experiment reproduced the initial behavior, confirming that the low apparent GRC effectiveness of PtNano is inherent to the catalyst configuration rather than the result of experimental irregularities. The poor GRC effectiveness is likely further aggravated by Pt particle agglomeration, as discussed in Section 3.1 and visible in Figure 4. SEM imaging reveals relatively large distances between Pt agglomerates, resulting in substantial membrane regions without direct Pt coverage. Consequently, parts of the crossover flux may pass through the membrane without encountering catalytically active Pt sites, thereby limiting recombination activity. These findings also highlight that the manufacturing process has a substantial influence on the effectiveness of GRC layers. Using advanced manufacturing methods, such as those proposed by Xie et al.[4], the PtNano system could potentially achieve better performance through improved particle dispersion.

For PtNano, the apparent GRC effectiveness ranges between 0.93 and 0.73, showing a decreasing trend at higher current densities. This general trend is also observed for all other samples and is somewhat unexpected. Literature suggests that, particularly at low current densities, the oxygen concentration at the GRC layer may limit the recombination reaction.[15,22] Under high differential pressures, such an oxygen undersupply should be most pronounced at low current densities, because oxygen supersaturation at the anode decreases with decreasing current density, reducing the oxygen concentration at the GRC layer and potentially limiting recombination.[15] Since this limitation is not observed in the present results, oxygen availability does not appear to limit the recombination reaction for the material systems studied here in the low-current density region. However, this conclusion may not necessarily hold for other material systems as it primarily depends on the anode electrode and the oxygen supersaturation.

A stronger contribution from HOR or chemical recombination

View Article Online
DOI: 10.1039/D6EY00106H



at the anode catalyst or PTL coating can also be excluded as an explanation for the increased recombination effectiveness at low current densities, since the current density dependence of these effects is already accounted for by normalizing to the reference apparent crossover flux. The general decrease in effectiveness at higher current densities can therefore be attributed to the overall increase in hydrogen crossover with increasing current density, which exceeds the GRC layer's capacity for complete recombination. However, this effect is less critical at high current densities because the dilution effect leads to generally low hydrogen in oxygen values. Consequently, effective recombination is most important at low current densities. A condition that is met for the samples investigated in this study.

Next, the PtBlack sample is considered. Overall, its reduction of the net detectable hydrogen content is high, with hydrogen in oxygen values of 0.32 vol.% at 0.25 A $cm^{-2}$, substantially surpassing the apparent GRC effectiveness of the PtNano sample. This result is somewhat unexpected, as the amount and spatial distribution of Pt clusters appear comparable to those of the PtNano sample (see Figure 4). However, as summarized in Section 1 of the SI, the PtBlack system exhibits a comparatively high specific surface area despite its large agglomerate size, which is attributed to its porous and highly roughened Pt morphology. Due to this rough surface morphology of the larger Pt particles, PtBlack proves to be an effective GRC system, achieving GRC effectiveness values $> 94\%$ across the entire current density range. In contrast to the PtNano catalyst, which consists of comparatively smooth spherical Pt particles with lower accessible surface area, the porous PtBlack morphology likely provides a substantially larger catalytically accessible Pt surface. This observation suggests that individual Pt particles may possess a relatively large "catchment area" for the recombination reaction. The size of this region could depend on the structure and surface properties of the platinum.

Under BoT conditions, the Pt/C system exhibits the highest reduction of the net detectable hydrogen content among the investigated GRC materials, achieving hydrogen in oxygen concentrations below 0.14 vol.% across the entire current density range and an apparent GRC effectiveness exceeding 98%. To assess the robustness of this observation, an independent second experiment was conducted using a newly fabricated CCM. The second measurement reproduced the initial results, confirming that the high apparent GRC effectiveness of the Pt/C system is reproducible under the applied test conditions (see Figure S.28 in the SI).

The origin of this markedly high GRC effectiveness cannot be conclusively determined based on the present dataset. However, the comparative trends allow some constraints to be placed on possible contributing mechanisms.

Several mechanisms may contribute to the observed GRC effectiveness of the Pt/C system. First, the high dispersion of Pt on the carbon support provides a large accessible Pt surface area, which may enhance catalytic recombination activity. As summarized in Section 1 of the SI, the Pt/C catalyst exhibits the highest specific surface area values exceeding the surface area metrics of the unsupported PtNano and PtBlack systems. Second, carbon-containing layers have been reported to influence hydrogen crossover behavior, for example through partial blocking effects, as discussed for graphene-based barrier layers in the fuel cell literature.[14,42] Given the different morphology and structure of the carbon support used here, the extent to which such effects contribute remains uncertain, and this interpretation should therefore be regarded as a working hypothesis. Third, the presence of the carbon support may alter local transport pathways within the membrane, potentially increasing the probability that permeating species encounter catalytically active sites or introducing additional transport resistances. Finally, if electrochemical pathways involving the hydrogen oxidation reaction (HOR) contribute to recombination, the electronic conductivity of the carbon support could facilitate local charge transfer processes. However, these possible contributions cannot be separated based on the present dataset. In particular, the measurements do not directly demonstrate that the carbon support itself modifies local transport pathways. The high apparent GRC effectiveness of the Pt/C system is therefore interpreted as a system-level observation, while the individual carbon-related mechanisms remain hypothetical.

These contributions are not independent but are intrinsically coupled through local transport–reaction interactions within the membrane. In particular, the experimentally observed hydrogen in oxygen signal reflects the combined effect of catalytic recombination, transport limitations, and structural modifications of the membrane environment. As already mentioned in Section 2.3, a quantitative separation of these individual contributions requires a detailed reaction–diffusion modeling framework which is beyond the scope of the present work.

Consequently, the present analysis focuses on the overall GRC effectiveness as a system-level performance metric, which inherently captures all contributing processes without attributing the observed behavior to a single dominant mechanism.

Overall, the present results do not allow a distinct discrimination between individual contributions or identification of a dominant recombination pathway. Targeted experiments, such as the use of non-conductive supports or carbon-only interlayers, would be required to further disentangle these effects but are beyond the scope of this study.

Despite excellent BoT results, the long-term stability of the Pt/C system remains uncertain, particularly in light of the ex-situ images indicating that little to no Pt remains in the original GRC layer after 1,500 h (see Figure 4f). In this configuration, the carbon support is located close to the harsh anode environment, separated only by a thin protective membrane layer. Although the stability of pure Pt within the membrane near the anode has been demonstrated over several thousand hours[5,7], the durability of Pt/C under comparable conditions has yet to be validated for extended operating times. Furthermore, a recent study by Smith-Lewis and Litster, which investigated a Pt/C GRC layer in operando, showed that the carbon support is susceptible to carbon corrosion, particularly under ambient-pressure conditions.[26] Therefore, the next section examines the EoT data of the net detectable hydrogen content in the anode exhaust gas after 1,500 h of operation to assess the stability of each GRC system.

View Article Online
DOI: 10.1039/D6EY00106H



### 3.3.2 End of test hydrogen in oxygen data

In this subsection, the EoT hydrogen in oxygen data after 1,500 h of operation is analyzed. Figure 8 presents the EoT data in the same format as the BoT data discussed previously. For clarity, the corresponding BoT data are included to enable direct comparison and to highlight differences between the BoT and EoT states.

A first general observation is that all depicted quantities (hydrogen in oxygen concentration, apparent hydrogen crossover flux, and apparent GRC effectiveness) show substantial deviations between BoT and EoT for all samples. This clearly illustrates the importance of long-term hydrogen in oxygen measurements, as a significant temporal dependence must be expected.

Another key observation is that the reference sample exhibits a decrease in the measurable hydrogen in oxygen content over time, whereas an increase might have been anticipated, for example due to membrane thinning or cathode degradation. Although this behavior may appear unexpected, it is fully reproducible: the overall trend for the reference CCM is confirmed by repeated measurements, as shown in Figures S.24 and S.25 in the SI, where a second measurement likewise exhibits a decrease in the measurable hydrogen in oxygen content over time. This behavior is analyzed in more detail in the following section, where the time-resolved evolution provides further insight into the underlying mechanisms. In addition, the behavior of the apparent hydrogen crossover flux as a function of current density for the EoT reference CCM (Figure 8b) appears unusual, exhibiting a dip in the low–current density regime and an approximately constant apparent crossover flux at current densities above 1 A $cm^{-2}$. Typically, a monotonic increase in hydrogen crossover with increasing current density would be expected.[41] However, deviations from this trend have also been reported previously, for example by Bernt et al.[43] Importantly, the observed behavior is reproducible and consistent with the additional reference measurement shown in Figure S.24 in the SI.

In contrast, all GRC samples continue to exhibit the monotonic increase in apparent crossover flux with current density already observed in the BoT measurements. A possible explanation for the different behavior of the reference CCM at EoT is that conditioning processes at the cathode, combined with structural degradation, may lead to pore widening within the electrode structure. Consequently, mass-transport limitations and local gas supersaturation effects at higher current densities could become less pronounced, thereby suppressing the characteristic increase in apparent hydrogen crossover flux with increasing current density. In the low–current density regime, the remaining weak current-density dependence observed in the measurement data may additionally be obscured by the comparatively higher experimental uncertainty in this operating range, as well as by recombination effects within the anode compartment. In contrast, the GRC samples still exhibit the monotonic increase in apparent crossover flux, suggesting that the overall crossover behavior is dominated by the GRC layer and that the influence of cathode structural changes is therefore comparatively less significant.

Based on these findings, one might initially expect the GRC samples to exhibit the same overall decreasing trend in hydrogen in oxygen values over time as the reference CCM, given that both systems employ identical electrodes and membranes. Contrary to this expectation, all GRC samples exhibit a pronounced increase in hydrogen in oxygen values over time. This behavior is consistently observed for all GRC samples and is further reproduced by repeated measurements using a newly assembled CCM of a representative GRC system (PtNano, see Figure S.27 in the SI). In combination with the decreasing trend observed for the reference CCM, these results strongly suggest that the increase in hydrogen in oxygen values in the GRC samples originates from a loss of GRC effectiveness rather than from structural changes in the electrodes or the membrane. If structural degradation of the cathode were responsible, a comparable trend would also be expected for the reference CCM. A key difference between the GRC and reference configurations is the substantially lower oxygen flux to the cathode in the GRC samples. However, there is no evidence supporting a causal relationship between increased oxygen availability at the cathode and the reduction in measurable hydrogen in oxygen values observed over time for the reference samples. The loss of apparent GRC effectiveness is further illustrated in Figure 8c. After accounting for the reduced EoT hydrogen crossover of the reference CCM, the decline in GRC effectiveness from BoT to EoT becomes clearly apparent.

A loss of recombination activity on the anode catalyst layer or on the coating of the anode PTL could, in principle, also explain the observed increase in measurable hydrogen in oxygen content over time. However, such effects would likewise occur in the reference CCM and would therefore already be reflected in the normalization using the reference data in Figure 8c. Consequently, these mechanisms alone cannot account for the behavior observed in the GRC samples. Instead, four possible mechanisms for the reduced recombination effectiveness of the GRC layers are proposed: i) Migration of GRC material (particles or ions) within the membrane toward less favorable or inactive sites for the recombination reaction, supported by the ex-situ images of the Pt/C sample (Figure 4f and Figure 5). ii) Oxidation of Pt particles in the GRC layer, altering their recombination activity. iii) Agglomeration of GRC material, reducing the available active surface area. iv) A decrease in oxygen crossover, leading to reduced oxygen availability at Pt sites and consequently lower recombination rates. This behavior is analyzed in more detail in the following section, where the time-resolved evolution provides further insight into the underlying mechanisms.

The Pt/C sample presents an especially intriguing case. Despite the SEM cross-section indicating a near-complete absence of Pt at its original location within the GRC layer, the recombination performance at EoT remains unexpectedly high. Several hypotheses may explain this apparent discrepancy: First, Pt may have migrated to other sites within the membrane while still remaining catalytically active. This hypothesis is consistent with the SEM images, which reveal the presence of a band-like Pt-enriched region within the membrane. This redistribution may thus result in an increased overall Pt surface area when the redeposited Pt is finely dispersed throughout the membrane. However, prior work by Martin et al. demonstrated that recombination layers are most effective when situated close to the anode, implying that Pt relo-

View Article Online
DOI: 10.1039/D6EY00106H



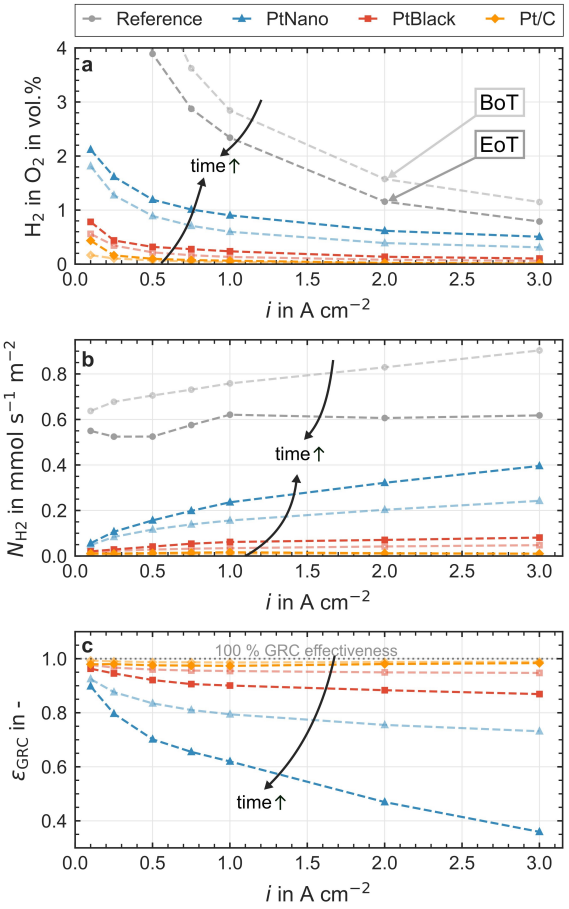


Fig. 8 Comparison of gas analysis data at BoT and EoT, measured at 80 °C and 30 bar absolute cathode pressure: (a) dilution-corrected measurable hydrogen in oxygen concentration at the anode outlet; (b) apparent hydrogen flux derived from the anode exhaust gas; (c) apparent GRC effectiveness, defined as $\varepsilon_{GRC} = 1 - N_{H2}^{cross}/N_{H2,ref}^{cross}$ (Eq. 1). BoT data from Fig. 7 are replotted for direct comparison.

cated away from this region would be expected to exhibit significantly reduced activity.[22] Second, the carbon support itself may continue to act as an effective blocking layer, although the extent to which carbon in this morphology can mitigate hydrogen crossover remains uncertain. Third, carbon may contribute directly to recombination activity. Previous studies have shown that carbon-based materials are capable of facilitating the gas recombination reaction, and Martin et al. further demonstrated that carbon PTLs can exhibit a measurable influence on recombination-driven reduction of the hydrogen in oxygen values in the anode exhaust stream.[44–46] In addition, the carbon support may contain surface defects, which could hypothetically further enhance the intrinsic catalytic activity of the carbon material.[47,48] Fourth, small residual Pt deposits on the carbon support (below the detection limit of SEM–EDX or masked by noise) may still be present and sufficient to sustain recombination. And lastly, ruthenium originating from the anode catalyst layer and deposited on the carbon matrix of the Pt/C sample may also contribute to gas recombination (see Figure S.5 in the SI). However, as discussed in Section 3.1, a significant contribution of ruthenium is considered unlikely, as it is detected only locally in the EoT GRC samples and does not form a continuous or homogeneous distribution across the carbon matrix.

In addition, the observation that the Pt/C sample maintains high recombination effectiveness at EoT, despite the apparent relocation of Pt away from its initial carbon-supported structure, suggests that the electronic conductivity of the carbon support alone is unlikely to fully explain the strong BoT performance of Pt/C-based GRC layers. Since it is observed that the recombination activity remains high even when the Pt is no longer located within the conductive carbon matrix, other factors may dominate the performance. This observation also raises the possibility that Pt migration may not necessarily constitute a detrimental degradation pathway for GRC layers, as recombination effectiveness can remain high even after substantial Pt relocation. This apparent discrepancy highlights that the relationship between Pt spatial distribution and recombination performance is not straightforward. However, the present data do not allow discrimination between these possibilities. Furthermore, it should be emphasized that the present experiments do not provide direct evidence for carbon-assisted recombination pathways or carbon-mediated enhancement of local transport processes. The carbon-related effects discussed above should therefore be regarded as possible explanations for the observed behavior rather than as experimentally confirmed mechanisms. Dedicated experiments, such as carbon-only interlayers, non-conductive supports, or spatially resolved operando measurements, would be required to isolate and quantify such contributions.

Overall, the GRC layers appear reasonably stable with respect to their ability to reduce the measurable hydrogen in oxygen values in the anode exhaust stream, since even after 1,500 h of stressed operation they still provide substantially lower values compared to the reference sample without a GRC layer. Notably, the Pt/C and PtBlack systems perform particularly well at EoT. Hence, the hypothesis that the Pt/C GRC layer would degrade rapidly due to the carbon support being located close to the harsh

View Article Online
DOI: 10.1039/D6EY00106H



anode environment cannot be confirmed under the test conditions and duration applied here. This behavior may be related to the high cathode pressures used in this study, as a recent publication indicated that at elevated cathode pressures the electric potential at the GRC layer remains close to zero and hence below the reversible potential for carbon corrosion.[26] Nevertheless, the present 1,500 h results, while indicating reasonable short-term stability, do not allow reliable conclusions regarding stability over substantially longer operating durations (e.g., several 10,000 h) that better reflect PEM system lifetime targets.[49]

Figure 8, however, does not resolve the temporal evolution of apparent hydrogen crossover over the 1,500 h test period. A central question therefore remains as to when during the test the observed increase occurred and how it may evolve further: Is the system approaching saturation, or is it still in an accelerating phase? To address this question, the next section examines the time-resolved evolution of measurable hydrogen in oxygen values to determine whether the observed trend originates from true degradation or from other effects, such as run-in behavior.

### 3.4 Time-resolved cell behavior during long-term stress test

This section analyzes the time-resolved evolution of the measurable hydrogen in oxygen values during the stress test. In addition, the temporal development of the open-circuit voltage (OCV) decay is examined, as a correlation with the evolution of the apparent hydrogen crossover is observed in the present dataset. Further time-dependent electrochemical data were recorded but are provided in the SI, as the focus of this work is placed on the effectiveness of different GRC configurations in reducing the net detectable hydrogen content in the oxygen outlet. However, if clear correlations between the electrochemical and gas analysis data can be identified, these are also identified and analyzed.

#### 3.4.1 Temporal progression of the measurable hydrogen in oxygen data

Figure 9 shows the temporal evolution of the measured hydrogen in oxygen content for all GRC samples at a current density of 0.25 A $cm^{-2}$. The corresponding data at 3 A $cm^{-2}$ are provided in Figure S.14 in the SI. The hydrogen in oxygen values were obtained during the constant current phase of the stress phase within the measurement protocol.

Based on these results, the temporal progression can be divided into two distinct phases: i) an initial run-in phase during the first 250 h, characterized by pronounced changes in the measured hydrogen in oxygen content, and ii) a subsequent regime, in which all samples exhibit only minor increases or decreases in hydrogen in oxygen values. This time-dependent behavior is consistently observed across all samples and is also reproduced in the reference and PtNano repeat measurements presented in the SI (see Figures S.25 and S.27). The temporal behavior for the GRC samples is illustrated more clearly in Figure 9b, where the data are shown in a zoomed-in representation, as the higher values of the reference data in Figure 9a obscure the detailed analysis of the GRC samples.

Regarding phase (i), similar behavior has been reported previously in the literature. For instance, Anschütz et al.[27] and Klose et al.[3] observed pronounced changes in hydrogen crossover during the first few hundred hours of operation. Anschütz et al. additionally identified a saturation effect similar to that observed here, whereas Klose et al. did not, likely because their experiment was terminated before saturation occurred. However, both studies employed experimental conditions that differ markedly from those in the present work, particularly with respect to cathode pressure and material set. A further noteworthy difference is that Anschütz et al. reported an increase in hydrogen crossover in the absence of a GRC layer, whereas the present reference sample without a GRC layer exhibits a decrease during the run-in period. By contrast, all samples containing a GRC show an increase in measurable hydrogen in oxygen values during phase (i), approximately doubling the hydrogen in oxygen content. Notably, this increase occurs over the same time scale as the decrease observed for the reference sample.

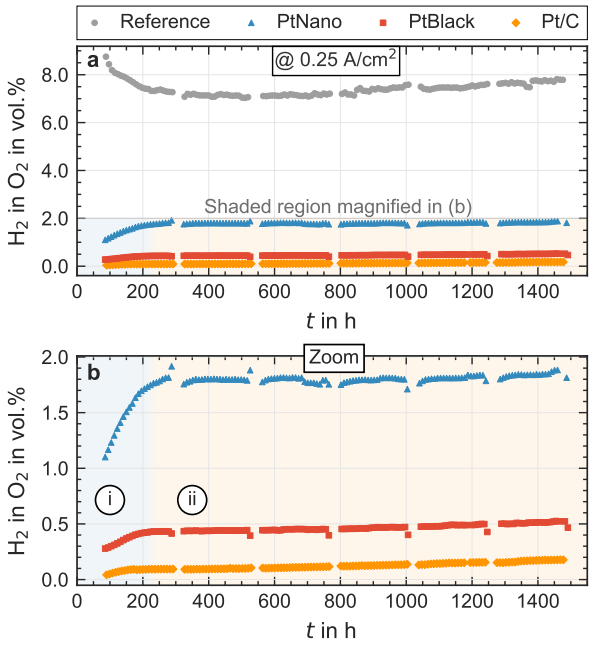


Fig. 9 Temporal evolution of the measurable hydrogen in oxygen concentration for all samples at 80 °C and 30 bar absolute cathode pressure: (a) full time series and (b) magnified view of the shaded region during the 0.25 A $cm^{-2}$ phase of the stress protocol. Corresponding data at 3 A $cm^{-2}$ are shown in Figure S.14 of the SI.

To rationalize the pronounced run-in behavior and, in particular, the opposing trends observed for the reference and GRC-containing samples, the reference case is considered first, as it is not influenced by a GRC layer and therefore reflects only electrode- and membrane-related effects. The observed decrease in measurable hydrogen in oxygen content during phase (i) can most probably not be explained by cathode degradation, as such degradation would be expected to increase the hydrogen in oxygen content due to enhanced supersaturation effects.

One possible explanation could be the migration of Pt from the cathode into the membrane, potentially forming an in-situ recombination layer that reduces the hydrogen-in-oxygen con-

View Article Online
DOI: 10.1039/D6EY00106H



tent at the anode. However, this mechanism appears unlikely, as Pt transport would have to occur against the prevailing electric field. While minor diffusion of Pt into the membrane cannot be excluded, it is expected to remain localized near the cathode and therefore would not provide an effective recombination sink for permeating hydrogen. An additional hypothesis is that carbon corrosion within the cathode leads to a widening of the pore structure, thereby facilitating the transition of hydrogen from the dissolved phase into the gaseous phase, which can then be more easily transported through the pores. This enhanced mass transport could potentially result in reduced apparent crossover fluxes.

A more plausible explanation is an initial conditioning of the cathode. Residual contaminants originating from manufacturing or assembly may initially enhance the measurable hydrogen in oxygen content and are gradually removed during operation. This interpretation is consistent with the electrochemical data, which also exhibit a decreasing trend during the initial phase. In addition, the observed decrease may not necessarily reflect a reduction in the actual crossover flux reaching the anode, but rather a change in the detectable fraction at the anode outlet. For instance, increasing recombination activity at the anode catalyst layer or within the PTL, potentially caused by structural rearrangements such as CCM creep into the PTL or morphological changes within the anode, may reduce the measurable hydrogen signal over time.

In principle, a similar behavior would be expected for the GRC-containing samples, as they share identical electrodes and largely identical membrane materials. However, the experimentally observed increase in hydrogen in oxygen content indicates that an additional, GRC-specific mechanism dominates the overall behavior. Since electrode-related effects are expected to evolve similarly to the reference case, the deviation must originate from changes in the recombination efficiency of the GRC layer.

The increase in measurable hydrogen in oxygen content during phase (i) can therefore be interpreted as a reduction in recombination effectiveness occurring on a similar time scale as the conditioning processes in the reference sample. As a result, the net observable signal is governed by the superposition of both effects.

A likely explanation for the reduced recombination effectiveness is a structural evolution of the membrane, such as swelling or deformation, which alters the effective transport pathways. This may lead to the formation of preferential pathways that bypass Pt particles, increasing the fraction of hydrogen permeating through the membrane without recombination. In contrast, a limitation due to reduced oxygen availability at the GRC layer appears unlikely, as no indication of oxygen limitation is observed.

Overall, the opposing trends observed during the run-in phase suggest that the temporal evolution of the GRC layer itself governs the initial increase in measurable hydrogen in oxygen content.

Regarding phase (ii), the hydrogen in oxygen values remain comparatively stable across all samples. Nevertheless, Figure 9b reveals that a slight but persistent increase in hydrogen in oxygen content is still observable for the GRC samples. Among them, the PtNano sample exhibits the lowest apparent degradation rate during phase (ii), at approximately 0.035 vol.% per 1,000 h, whereas Pt/C and PtBlack show higher and nearly identical rates of 0.073 and 0.071 vol.% per 1,000 h, respectively. Notably, the hydrogen in oxygen content of the reference sample also begins to increase after approximately 600 h of operation, indicating that degradation mechanisms such as membrane thinning or cathode degradation start to dominate once the initial run-in effect with a decreasing hydrogen in oxygen trend starts to subside. Consequently, the increase in hydrogen crossover flux detectable in the anode exhaust stream observed for the GRC samples during phase (ii) cannot be attributed exclusively to degradation of the GRC layer but rather reflects the combined degradation of multiple system components, including the membrane and electrodes.

Assuming that the observed degradation rates of the GRC samples remained constant and applying an assumed shutdown limit of 1 vol.% hydrogen in oxygen, the PtNano sample would already exceed this threshold and therefore would not be considered operable under the conditions of phase (ii). In contrast, the PtBlack and Pt/C samples would reach the assumed shutdown limit at a current density of 0.25 A $cm^{-2}$ only after approximately 8,400 h and 12,800 h of operation, respectively. Beyond these estimated shutdown times, additional mitigation measures such as reducing the operating pressure or restricting operation to higher current densities than 0.25 A $cm^{-2}$ would be required. However, it should be emphasized that these estimates are derived from our measurement protocol which was designed to accelerate degradation. Hence, this lifetime estimation is intended solely as a theoretical, order-of-magnitude illustration to contextualize the observed evolution of measurable hydrogen in oxygen values. For this purpose, a linear regression of the hydrogen in oxygen data during phase (ii) was used to estimate an average degradation rate, which was then extrapolated under the simplifying assumption that this rate remains constant. This approach does not imply that the temporal evolution of measurable hydrogen in oxygen values can be described by linear interpolation, nor that the observed trend will persist over extended operation. It remains highly uncertain whether the increase in hydrogen in oxygen content would decelerate, remain stable, or accelerate with continued operation. Accordingly, the extrapolated shutdown times should be regarded as purely indicative rather than predictive. Nevertheless, this analysis clearly demonstrates that the hydrogen in oxygen content can evolve significantly over time and may approach critical thresholds that constitute a shutdown criterion for safety reasons. In the hypothetical case that the observed phase (ii) behavior were to continue, the estimated times to reach the assumed shutdown limit of 1 vol.% would remain far below lifetime targets exceeding 50,000 h.[49] This highlights the necessity of explicitly monitoring hydrogen in oxygen values over extended test durations, particularly when GRC layers are incorporated into the membrane, as their temporal evolution is difficult to predict yet directly relevant for safe and reliable operation.

In summary, the majority of the changes in the measurable hydrogen in oxygen content between BoT and EoT presented in Section 3.3.2 occur within the first 250 h for all samples. This behavior is therefore interpreted primarily as an initial conditioning or run-in process rather than true degradation, consistent with

View Article Online
DOI: 10.1039/D6EY00106H



trends reported in the literature.[27] The onset of actual degradation appears only after this initial period and manifests as a significantly slower increase in measurable hydrogen in oxygen content. During this later phase, degradation rates are clearly reduced. However, a continued increase in hydrogen in oxygen content remains observable. The key question is whether this aging will continue in a steady linear progression, eventually accelerate, or perhaps decelerate. Addressing this question requires even longer measurements in the order of 10,000 h to reliably assess the stability of these systems.

### 3.4.2 Temporal development of OCV decay curves

In addition to the measurable hydrogen in oxygen values, the temporal evolution of the open-circuit voltage (OCV) decay is analyzed. The time-dependent changes observed in the OCV decay curves exhibit trends similar to those of the hydrogen in oxygen measurements, motivating a more detailed investigation of the OCV behavior. First, an overview of the OCV decay characteristics is presented, followed by a comparison of OCV data obtained for samples with and without GRC layers.

During the OCV phases, open-circuit conditions are applied, under which no electric current flows, and the cell voltage decay is monitored for 300 s. These OCV phases were originally implemented as a stressor and are therefore an integral part of the recurring stress phase in the test protocol, as shown in Figure 3. As a result, repeated voltage decay profiles during the OCV phase are available for each sample, enabling an analysis of the temporal progression of the OCV decay over the full 1,500 h test duration. Figure 10 illustrates the voltage decay during these five-minute OCV periods and its evolution over time, visualized using the color scale.

The BoT OCV curve, indicated in dark purple, is considered first. All samples exhibit a similar pattern at BoT: an initial slow and approximately linear voltage decay followed after a distinct turning point by a rapid voltage drop. This characteristic pattern is consistently observed across all samples. However, transferring this behavior to other studies is challenging because OCV characteristics are strongly influenced by the specific setup and operating conditions. For example, Krenz et al.[50] reported a more linear or constant voltage decay for a system without a GRC layer operated at ambient pressure, while Brightman et al.[51] used a reference electrode and observed yet another distinct voltage profile. Overall, a variety of processes could influence OCV behavior and give rise to the pattern observed here. Several such mechanisms are discussed below.

A plausible mechanism for the slow voltage decay in the initial part of the curve is the gradual discharge of the double layer combined with slow hydrogen and oxygen crossover driven by concentration gradients. The subsequent rapid voltage drop may occur once oxygen at the anode becomes depleted, such that hydrogen crossing over from the high-pressure cathode increasingly dominates the anode gas composition. Ultimately, the cell approaches a voltage close to 0 V in all cases, consistent with both electrodes becoming fully saturated with hydrogen if we can assume that the cathode stays around 0 V due to a persistent hydrogen atmosphere.

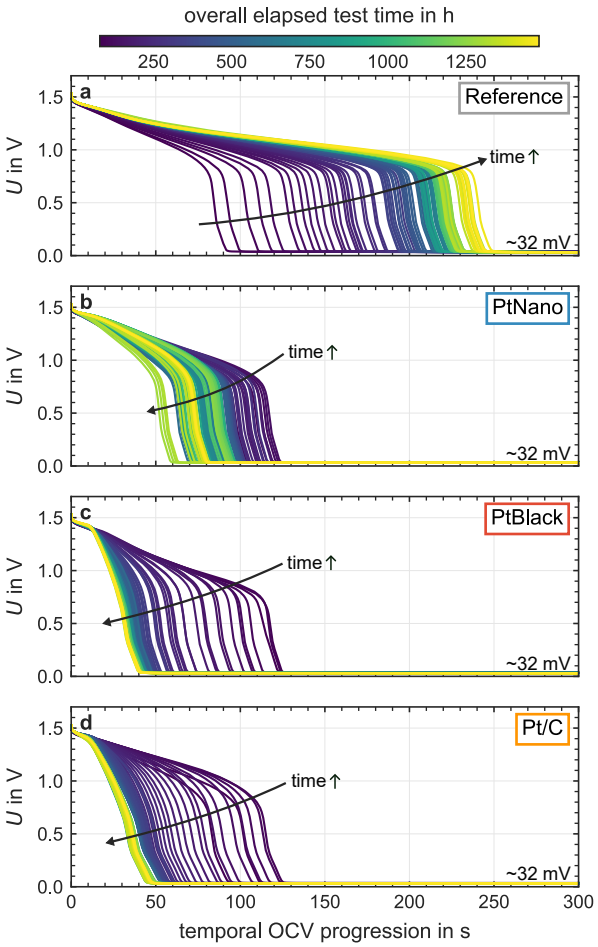


Fig. 10 Temporal evolution of the voltage decay following a switch from 1.5 V to open-circuit conditions for all samples at 80 °C and 30 bar absolute cathode pressure during the stress phase with a continuous water circulation on the anode side.

View Article Online
DOI: 10.1039/D6EY00106H



The role of GRC layers within the membrane in shaping OCV behavior remains relatively unexplored in PEM water electrolysis. Several possible influences can be identified. The presence of platinum within the membrane may facilitate short-circuit currents, potentially accelerating charge balancing. In addition, it is well established that the concentrations of hydrogen and oxygen at the electrodes influence the overall cell potential. Consequently, crossover fluxes also affect the voltage response during the OCV phase. As the GRC layer alters local gas concentrations and crossover fluxes, it is therefore expected to influence the potential evolution during the OCV phase. This influence may arise because, with the GRC layer positioned near the anode, oxygen is depleted more rapidly due to recombination, thereby increasing the concentration gradient that drives oxygen removal.

When comparing the OCV profiles of the different samples and their evolution over 1,500 h, a clear pattern emerges. At BoT, the curves appear highly similar across all samples. In particular, the onset of the abrupt voltage drop consistently occurs between approximately 100 and 130 s, irrespective of whether a GRC layer is present. With increasing test duration, however, differences between the samples become more pronounced. The reference sample without a GRC layer shows a progressively "slower" OCV decay (shifted to the right), whereas the voltage equalization time for all samples with a GRC layer becomes faster and shifts to the left. Notably, this behavior correlates with the temporal development of the hydrogen in oxygen data in Figure 9: only the reference sample exhibits an initial decrease in hydrogen in oxygen content over time, whereas all GRC-containing samples show an increase. The time scales are consistent as well: both effects primarily originate in the first 250 h, after which a more stable behavior is observed. This suggests a possible interdependence between the two phenomena (temporal change in OCV curve and hydrogen crossover run-in effect) or a common underlying mechanism, although a direct causal relationship cannot be conclusively established based on the present data alone. A potential influence of cathode pressure e.g., through leakage or varying rates of pressure decay can be ruled out, as Figure S.13 in the SI shows uniform pressure levels across all samples throughout the OCV phases.

It is also worth noting that the overall OCV behavior is quite similar for all GRC samples, despite substantial differences in absolute hydrogen in oxygen values during electrolysis operation. This suggests that the apparent GRC effectiveness of the GRC layer does not strongly influence the shape of the OCV decay curve. Instead, the mere presence of a GRC layer appears to be the dominant factor. One plausible explanation is that the GRC layer becomes inactive shortly after the onset of OCV, once the available oxygen in the anode catalyst layer has been consumed or displaced by hydrogen from the cathode. Furthermore, this observation suggests that the Pt redistribution within the membrane does not have a substantial influence on the OCV behavior. This interpretation is supported by the fact that similar OCV decay characteristics are observed for all GRC samples, despite pronounced Pt redistribution being detected only in the Pt/C system. Consequently, the Pt redistribution is likely not a dominant factor governing the OCV response.

Although these observations raise several open questions that cannot yet be fully resolved, they may offer valuable insight for future studies. In particular, the distinct evolution of OCV profiles could be relevant for practical applications, where monitoring OCV behavior in operating systems may provide a useful, non-invasive diagnostic indicator of system health or change in material properties during operation.

## 4 Conclusion and Outlook

This work provides a systematic, time-resolved comparison of different platinum-based GRC configurations operated for 1,500 h under industrially relevant high-pressure conditions. Although all samples exhibited comparable electrochemical performance and overall stability, distinct differences in the reduction of the net detectable hydrogen content in the oxygen outlet were observed, despite identical platinum loadings within the GRC layer. This finding indicates that long-term evolution of the hydrogen in oxygen data and the associated performance evolution depend primarily on the specific Pt catalyst configuration rather than on Pt loading alone. Among the investigated GRC samples (PtNano, PtBlack, and Pt/C), the Pt/C configuration demonstrated the most substantial reduction in measurable hydrogen in oxygen in the anode exhaust stream. This behavior is consistent with the large accessible Pt surface area of the Pt/C catalyst. Additional effects related to the carbon support, such as modified local transport pathways or altered transport–reaction interactions, may also contribute. However, the present experiments do not provide direct evidence for carbon-assisted recombination or carbon-mediated transport enhancement, and these possible contributions cannot be separated from Pt-related effects based on the available data. While the measurable hydrogen in oxygen values of the other two GRC samples were substantially lower than that of the reference without GRC, it remained inferior to the Pt/C sample. This performance gap could possibly be reduced through optimization of the manufacturing process of the PtBlack and PtNano sample, for example by mitigating agglomeration effects.

A key finding of this study is post-mortem evidence for pronounced changes in the Pt spatial distribution within membrane-integrated GRC layers, as revealed by SEM–EDX cross-sections. For the Pt/C system, SEM–EDX indicates a strong depletion of Pt at the initial GRC layer position after 1,500 h, accompanied by the occurrence of a distinct band-like Pt-enriched region within the membrane. Although the resolution limitations of SEM–EDX prevent equally clear conclusions for the PtNano and PtBlack samples, the absence of comparable features does not preclude the occurrence of similar redistribution processes at lower rates or below the detection limit. A possible explanation is the higher fraction of small, highly accessible Pt particles in Pt/C, which may increase dissolution susceptibility and Pt mobility compared with the larger and more agglomerated Pt structures in PtBlack and PtNano. These observations point to material-dependent differences in the structural evolution of membrane-integrated GRC layers, highlighting the role of both catalyst and support structure in long-term stability.

Unexpectedly, the Pt/C system maintains a strong reduction in measurable hydrogen in oxygen values despite the apparent re-

View Article Online
DOI: 10.1039/D6EY00106H



distribution of Pt away from its initial GRC layer position. This observation may be consistent with catalytically active Pt remaining effective after redistribution within the membrane, residual Pt below the SEM-EDX detection limit, or possible carbon-related contributions associated with the carbon matrix that largely remains at the original position. However, the present data do not allow these mechanisms to be distinguished, and carbon-assisted recombination or carbon-mediated transport effects can only be regarded as possible explanations rather than experimentally confirmed mechanisms. These observations suggest that effective recombination is not necessarily confined to the initially defined GRC layer position and that substantial GRC restructuring does not inherently result in performance losses with respect to reducing the amount of hydrogen reaching the anode side.

Across all investigated GRC systems, the measurable hydrogen in oxygen content increases predominantly during the first 250 h of operation before transitioning into a slow-aging regime. This behavior identifies an early-life run-in phase that dominates the overall evolution of apparent hydrogen crossover over time. The strong correlation between this run-in behavior and the evolution of the OCV decay suggests that OCV characteristics may serve as a practical diagnostic indicator for changes in hydrogen crossover or its consequences, i.e. changes in the electrode structures in real electrolyzer systems.

Overall, this study establishes that (i) the reduction of the net detectable hydrogen content in the oxygen outlet by Pt-based GRC layers depends strongly on the catalyst configuration and not only on the amount of catalytic material, (ii) material-specific degradation and restructuring pathways exist, (iii) Pt within membrane-integrated GRC layers can undergo redistribution, resulting in previously unreported band-like Pt-enriched regions within the membrane, and (iv) low measured hydrogen in oxygen values can persist despite significant structural changes in the GRC layer. Taken together, these findings provide a basis for the further development of resource-efficient and durable GRC concepts for safe high-pressure PEM water electrolysis.

To build on these findings, future work is currently underway and will focus on high-resolution mapping of Pt transport pathways (e.g., synchrotron XRF or TEM–EDX tomography) to clarify the mechanisms behind the observed band-like Pt accumulation. Such studies are required to distinguish between possible mechanisms such as Pt dissolution, electrochemical transport of Pt-containing ionic species, chemically driven diffusion, and redeposition processes, which may have different implications for long-term durability. In addition, complementary operando studies are needed to determine whether Pt remains catalytically active after migration and to disentangle the contributions of chemical recombination, HOR, and potential carbon-assisted pathways. To validate long-term viability, extended durability studies exceeding 10,000 h are essential, particularly for Pt/C systems, where long-term stability remains uncertain due to the Pt redistribution observed here. Finally, the observed link between hydrogen crossover evolution and OCV behavior should be investigated in more detail, as it may enable the development of diagnostic approaches exploiting OCV decay as a real-time health indicator in industrial PEM electrolyzers.

## Author contributions

**Steffen Brundiers:** conceptualization, methodology, software, validation, formal analysis, investigation, data curation, writing - original draft, writing—review & editing, visualization. **Patrick Trinke:** conceptualization, methodology, validation, writing—review & editing, supervision. **Simon Geiger:** conceptualization, resources, writing—review & editing. **Victor-Alfonso Gracia-Medrano-Bravo:** resources, writing—review & editing. **Marek Hubka:** resources, writing—review & editing. **Jan Ilsemann:** conceptualization, resources, writing—review & editing. **Boris Bensmann:** conceptualization, methodology, validation, writing—review & editing, supervision. **Richard Hanke-Rauschenbach:** conceptualization, writing—review & editing, supervision.

## Conflicts of interest

There are no conflicts to declare.

## Data availability

The data supporting the findings of this study are available in the Supplementary Information (https://doi.org/XXXX.). The complete set of original measurement data is openly available via the Zenodo repository at https://doi.org/10.5281/zenodo.19361280.

## Acknowledgements

The authors thank Torben Gottschalk for the design and building of the test bench, Nils-Eric Rahm for the design of the test cell, Sven Wiegelmann for the original code of the SI files, and Christoph Andreas Löcherer for the fruitful discussion regarding the OCV behavior. The authors additionally acknowledge the financial support by the Federal Ministry of Research, Technology and Space of Germany in the framework of evolver (03SF0765) as well as HyThroughGen (03HY108C), and thank the Institute for Solar Energy Research Hamelin (ISFH) for the coating of the PTLs.

## References

1 Z. Zhang, Z. Han, A. Testino and L. Gubler, *J. Electrochem. Soc.*, 2022, **169**, 104501.
2 A. Stähler, M. Stähler, F. Scheepers, W. Lehnert and M. Carmo, *J. Electrochem. Soc.*, 2022, **169**, 034522.
3 C. Klose, P. Trinke, T. Böhm, B. Bensmann, S. Vierrath, R. Hanke-Rauschenbach and S. Thiele, *J. Electrochem. Soc.*, 2018, **165**, F1271–F1277.
4 X. Xie, J. Song, X. Fan, W. Zhao, K. Liu, Y. Zhao, L. Zhou, Y. Xiao, S. Li, H. Wang, G. Zhao, F. Xie, B. Song, Q. Guo, X. Jiao, P. He, F. Liu and Y. Zhang, *Adv. Funct. Mater.*, 2025, **35**, 2504467.
5 G. Mirshekari, R. Ouimet, Z. Zeng, H. Yu, S. Bliznakov, L. Bonville, A. Niedzwiecki, C. Capuano, K. Ayers and R. Maric, *Int. J. Hydrogen Energy*, 2021, **46**, 1526–1539.
6 Z. Zeng, R. Ouimet, L. Bonville, A. Niedzwiecki, C. Capuano, K. Ayers, H. Yu, R. Maric and S. Bliznakov, *Int. J. Hydrogen Energy*, 2025, **114**, 534–544.

View Article Online
DOI: 10.1039/D6EY00106H



7 R. J. Ouimet, H. Yu, G. Mirshekari, Z. Zeng, L. J. Bonville, S. Bliznakov, A. Niedzwiecki, P. Mani, C. Capuano, K. E. Ayers and R. Maric, *ECS Meet. Abstr.*, 2020, **MA2020-02**, 2469.

8 R. Omrani and B. Shabani, *Electrochim. Acta*, 2021, **377**, 138085.

9 M. Schalenbach, M. Carmo, D. L. Fritz, J. Mergel and D. Stolten, *Int. J. Hydrogen Energy*, 2013, **38**, 14921–14933.

10 M. Schalenbach and D. Stolten, *Electrochim. Acta*, 2015, **156**, 321–327.

11 S. A. Grigoriev, P. Millet, S. V. Korobtsev, V. I. Porembskiy, M. Pepic, C. Etievant, C. Puyenchet and V. N. Fateev, *Int. J. Hydrogen Energy*, 2009, **34**, 5986–5991.

12 H. Ito, N. Miyazaki, M. Ishida and A. Nakano, *Int. J. Hydrogen Energy*, 2016, **41**, 20439–20446.

13 P. Trinke, P. Haug, J. Brauns, B. Bensmann, R. Hanke-Rauschenbach and T. Turek, *J. Electrochem. Soc.*, 2018, **165**, F502.

14 P. Guan, M. Jiang, W. Li, W. Zhang, L. Zhang, K. Long, D. Yuan, T. Ma, D. Wang, H. K. Liu, S. X. Dou and Y. Dou, *Adv. Mater.*, 2025, e08400.

15 S. Brundiers, P. Trinke, B. Bensmann and R. Hanke-Rauschenbach, *J. Electrochem. Soc.*, 2024, **171**, 074509.

16 S. Garbe, E. Samulesson, T. J. Schmidt and L. Gubler, *J. Electrochem. Soc.*, 2021, **168**, 104502.

17 F. Pantò, S. Siracusano, N. Briguglio and A. S. Aricò, *Appl. Energy*, 2020, **279**, 115809.

18 N. Briguglio, F. Pantò, S. Siracusano and A. S. Aricò, *Electrochim. Acta*, 2020, **344**, 136153.

19 N. Briguglio, S. Siracusano, G. Bonura, D. Sebastián and A. S. Aricò, *Appl. Catal. B Environ.*, 2019, **246**, 254–265.

20 D. Hou, L. Liu, G. Qiao, X. Zhang, Y. Yan, Y. Li and S. Du, *Chem. Eng. J.*, 2025, **512**, 162524.

21 S. Garbe, U. Babic, E. Nilsson, T. J. Schmidt and L. Gubler, *J. Electrochem. Soc.*, 2019, **166**, F873–F875.

22 A. Martin, D. Abbas, P. Trinke, T. Böhm, M. Bierling, B. Bensmann, S. Thiele and R. Hanke-Rauschenbach, *J. Electrochem. Soc.*, 2021, **168**, 094509.

23 D. Abbas, A. Martin, P. Trinke, M. Bierling, B. Bensmann, S. Thiele, R. Hanke-Rauschenbach and T. Böhm, *J. Electrochem. Soc.*, 2022, **169**, 124514.

24 Z. Zhang, M. Sirim, D. Baster, M. El Kazzi, A. Testino and L. Gubler, *ACS Appl. Mater. Interfaces*, 2025, **17**, 54656–54667.

25 R. Zhang, Z. Yuan, X. Qiu, Z. Rui, X. Shi, J. Li, A. Tan and J. Liu, *J. Mater. Chem. A*, 2025, 32416–32426.

26 C. Smith-Lewis and S. Litster, *Int. J. Hydrogen Energy*, 2025, **196**, 152521.

27 L. Anschütz, M. Ise, T. Gottschalk, P. Trinke, B. Bensmann, R. Hanke-Rauschenbach and M. Suermann, *Int. J. Hydrogen Energy*, 2026, **203**, 153179.

28 S. Fahr, F. K. Engel, S. Rehfeldt, A. Peschel and H. Klein, *Int. J. Hydrogen Energy*, 2024, **68**, 705–721.

29 S. Brundiers, *Datasets: Time-Resolved Performance and Stability of Different Gas Recombination Catalysts in PEM Water Electrolysis*, 2026.

30 R. P. M. Duarte, A. Kowal, J. Young, J. T. Lang, I. Zenyuk, J. A. Wrubel and G. Bender, *Int. J. Hydrogen Energy*, 2025, **165**, 150924.

31 A. Martin, P. Trinke, B. Bensmann and R. Hanke-Rauschenbach, *J. Electrochem. Soc.*, 2022, **169**, 094507.

32 A. T. S. Freiberg and S. Thiele, *J. Electrochem. Soc.*, 2025, **172**, 034506.

33 R. Gawas, D. I. Kushner, X. Peng and R. Mukundan, *Energy Environ. Sci.*, 2025, **18**, 4625–4631.

34 T. Jahnke, G. A. Futter, A. Baricci, C. Rabissi and A. Casalegno, *J. Electrochem. Soc.*, 2019, **167**, 013523.

35 W. Bi, G. E. Gray and T. F. Fuller, *Electrochem. Solid-State Lett.*, 2007, **10**, B101.

36 S. F. Burlatsky, M. Gummalla, V. V. Atrazhev, D. V. Dmitriev, N. Y. Kuzminyh and N. S. Erikhman, *J. Electrochem. Soc.*, 2011, **158**, B322.

37 G. J. B. Agravante and J. T. Gostick, *J. Electrochem. Soc.*, 2026, **173**, 074507.

38 L. Amichi, H. Yu, A. Ziabari, O. Rahman, D. Arregui-Mena, L. Hu, K. C. Neyerlin and D. A. Cullen, *Adv. Energy Mater.*, 2024, **14**, 2402310.

39 A. Rex, L. Almeida De Campos, T. Gottschalk, D. Ferreira Sanchez, P. Trinke, S. Czioska, E. Saraçi, B. Bensmann, J.-D. Grunwaldt, R. Hanke-Rauschenbach and T. L. Sheppard, *Adv. Energy Sustain. Res.*, 2024, **5**, 2400048.

40 E. Padgett, A. Adesso, H. Yu, J. Wrubel, G. Bender, B. Pivovar and S. M. Alia, *J. Electrochem. Soc.*, 2024, **171**, 064510.

41 P. Trinke, B. Bensmann and R. Hanke-Rauschenbach, *Int. J. Hydrogen Energy*, 2017, **42**, 14355–14366.

42 M. Komma, A. T. S. Freiberg, D. Abbas, F. Arslan, M. Milosevic, S. Cherevko, S. Thiele and T. Böhm, *ACS Appl. Mater. Interfaces*, 2024, **16**, 23220–23232.

43 M. Bernt, J. Schröter, M. Möckl and H. A. Gasteiger, *J. Electrochem. Soc.*, 2020, **167**, 124502.

44 A. Martin, P. Trinke, C. Van Pham, M. Bühler, M. Bierling, P. K. R. Holzapfel, B. Bensmann, S. Thiele and R. Hanke-Rauschenbach, *J. Electrochem. Soc.*, 2021, **168**, 114513.

45 H. Dietz, L. Dittmar, D. Ohms, M. Radwan and K. Wiesener, *J. Power Sources*, 1992, **40**, 175–186.

46 K. Waki, R. A. Wong, H. S. Oktaviano, T. Fujio, T. Nagai, K. Kimoto and K. Yamada, *Energy Environ. Sci.*, 2014, **7**, 1950–1958.

47 Y. Jia and X. Yao, *Acc. Chem. Res.*, 2023, **56**, 948–958.

48 L. Zhang, Q. Xu, J. Niu and Z. Xia, *Phys. Chem. Chem. Phys.*, 2015, **17**, 16733–16743.

49 T. Roeder, A. Rosenstiel, N. Monnerie and C. Sattler, *Int. J. Hydrogen Energy*, 2024, **95**, 1242–1251.

50 T. Krenz, A. Rex, L. Helmers, P. Trinke, B. Bensmann and R. Hanke-Rauschenbach, *J. Electrochem. Soc.*, 2024, **171**, 124501.

51 E. Brightman, J. Dodwell, N. van Dijk and G. Hinds, *Electrochem. Commun.*, 2015, **52**, 1–4.

View Article Online
DOI: 10.1039/D6EY00106H

**Data Availability:**

The data supporting the findings of this study are available in the Supplementary Information (https://doi.org/XXXX.). The complete set of original measurement data is openly available via the Zenodo repository at https://doi.org/10.5281/zenodo.19361280.